Mathematical Biosciences and Engineering

https://www.aimspress.com/journal/mbe

MBE, 22(9): 2300–2338.
DOI: 10.3934/mbe.2025084
Received: 31 March 2025
Revised: 19 May 2025
Accepted: 04 June 2025
Published: 17 July 2025

Research article

Impact of vaccination behavior on COVID-19 dynamics and economic outcomes

Abdallah Alsammani[1,*], Calistus N. Ngonghala[2,3,4,5] and Maia Martcheva[2]

[1] Department of Mathematics, Jacksonville University, Jacksonville, FL 32211, USA
[2] Department of Mathematics, University of Florida, Gainesville, FL 32611, USA
[3] Emerging Pathogens Institute, University of Florida, Gainesville, FL 32610, USA
[4] Harvard Radcliffe Institute of Advanced Studies, 10 Garden St., Cambridge, MA 02138, USA
[5] Department of Global Health and Social Medicine, Harvard Medical School, Boston, MA 02115, USA

* **Correspondence:** Email: aalsamm@ju.edu.

Abstract: COVID-19 is a highly transmissible respiratory disease that has significantly impacted global health and economies. In this study, we investigated the impact of immunity duration, vaccination behavior, transmission reduction measures, and healthcare timing and duration on COVID-19 dynamics and economic outcomes. Using a mathematical model that integrates epidemiological, human behavioral, and economic factors, we analyzed the effectiveness of interventions based on real-world data. Analytical results revealed up to six disease-free equilibria, with stability determined by reproduction number thresholds. Results from numerical simulations of the model indicated that prolonged immunity and high vaccination rates can reduce peak infections and deaths, whereas delayed hospitalizations and increased transmission can exacerbate outbreaks. Sensitivity analysis highlights vaccine efficacy and uptake as key determinants of disease control. These findings underscore the need for sustained vaccination, timely healthcare interventions, and strategic public health measures.

Keywords: COVID-19; economic impact; human behavior; public health interventions

1. Introduction

COVID-19 has had a profound health and economic impact on the US, leading to over a million deaths and long-term health complications for many survivors [1, 2]. Moreover, the pandemic overwhelmed healthcare systems, strained medical resources, and exacerbated existing health disparities [3, 4]. Economically, it triggered a sharp recession, causing widespread job losses,

business closures, and disruptions to global supply chains [5, 6]. Government interventions, including stimulus packages and emergency policies, mitigated some effects, but inflation, labor shortages, and economic uncertainty persisted. While vaccination efforts and public health measures have helped control the virus, the long-term consequences on healthcare, productivity, and economic stability remain significant.

In the US, COVID-19 vaccination efforts have used various vaccine types, including mRNA vaccines (Pfizer-BioNTech and Moderna), viral vector vaccines (Johnson & Johnson's Janssen), and protein subunit vaccines (Novavax) [7, 8]. These vaccines have demonstrated high efficacy in preventing severe illness, hospitalization, and death. For instance, mRNA vaccines have shown effectiveness rates up to 95% in clinical trials [9–11]. The widespread administration of these vaccines has significantly reduced COVID-19-related mortality and morbidity. However, challenges such as vaccine hesitancy persist, influenced by factors such as misinformation, distrust in healthcare systems, and concerns about potential side effects of vaccines [12–15]. Addressing vaccine hesitancy requires understanding individuals' decision-making processes and implementing effective risk communication strategies.

Human behavior has played a critical role in the pandemic's trajectory, as personal decisions regarding vaccination and adherence to public health measures have directly impacted the spread of the virus and the effectiveness of mitigation efforts. Individuals and communities assessed the costs and benefits of protective actions, often adjusting their behaviors based on observed outcomes and social influences. The costs of preventive measures included discomfort from mask-wearing, vaccine side effects, economic hardships, and mental health challenges from lockdowns, while the risks of inaction involved severe illness, long-term health complications, and death [16, 17]. The payoffs for adopting protective behaviors included reduced transmission, personal and community protection, and avoiding severe disease. Public perception, shaped by social norms and trust in institutions, influenced how people sampled others' behaviors and determined whether the perceived benefits outweighed the costs. This dynamic feedback loop between individual decision-making and collective behavior played a crucial role in shaping the course of the pandemic. Thus, understanding this interplay is essential for developing mathematical models to inform actionable and effective pandemic response strategies.

Mathematical modeling played a crucial role in the fight against COVID-19 and other infectious diseases, particularly in the early stages, by informing policy decisions, forecasting healthcare demand, and evaluating intervention strategies. For example, Ferguson et al. [18] presented projections of ICU demand and mortality under varying non-pharmaceutical interventions (NPIs), influencing public health policies in the UK. Ngonghala et al. [19–21] developed models to assess the impact of lockdowns, healthcare access, and testing rates on disease spread and healthcare burden. Gumel et al. [22] provided a primer to help public health officials interpret and apply epidemic modeling outcomes. These early efforts primarily focused on the role of NPIs such as social distancing, lockdowns, and contact reduction measures. As vaccines became available, researchers expanded their models to study the effects of vaccination strategies on pandemic dynamics [23–26]. Some studies examined the interplay between human behavior and disease spread, recognizing that individual compliance with health measures significantly influences outcomes [27, 28]. For instance, Ngonghala et al. [27] developed models that incorporate behavioral fatigue and perceived risk, showing how these factors dynamically affect compliance with interventions. Martcheva et al. [28]

introduced a game-theoretic framework for vaccination behavior, illustrating feedback between individual decision-making and epidemic dynamics. A study published in *Nature Human Behaviour* [17] emphasized the role of social and behavioral sciences in promoting public adherence to interventions during the pandemic. Additionally, Banholzer et al. [29] explored how NPIs and vaccination policies influence economic activity, offering a model-based analysis of their macroeconomic impacts. Despite these contributions, relatively few models, such as that by Martcheva et al. [28] have simultaneously addressed the combined effects of human behavior, economic outcomes, and disease dynamics. This underscores the need for integrated approaches to inform balanced public health and economic policies.

Additionally, researchers have explored the interactions between COVID-19 and the economy, analyzing how NPIs and vaccination efforts affect economic activity. A study in *PLoS One* [29] modeled the economic implications of various NPIs, providing insights into balancing public health and economic interests. However, relatively few models, including those by Martcheva et al. [28] have simultaneously addressed the combined effects of human behavior, economic factors, and disease dynamics, underscoring the need for comprehensive approaches to inform policy decisions.

In this study, we develop a mathematical model that integrates the epidemiology of COVID-19, human behavioral responses to vaccination, and their combined effects on economic growth. Unlike traditional models that separately examine disease spread, vaccination dynamics, or economic impact, this framework captures the feedback loop between disease dynamics, individual vaccination decisions, and economic performance. Parameterized with daily COVID-19 case and mortality data from the US, the model is used to evaluate how varying immunity durations, hospitalization timing and duration, transmission reduction interventions, vaccine efficacy, and coverage, as well as behavioral shifts in vaccine uptake, influence COVID-19 trajectories and economic stability. Incorporating adaptive human behavior and resource constraints provides a more comprehensive understanding of pandemic dynamics and informs policies for balancing public health and economic recovery. The rest of the paper is structured as follows: In Section 2 we develop the mathematical model, with analytical results in Section 3. Model fitting and identifiability analysis are in Section 4, while in Section 5, we present numerical simulations, including sensitivity analyses. In Section 6, we discuss the findings and conclusions.

2. Model formulation

In this section, we introduce a COVID-19 vaccination model. We split the total population at time t, denoted by $N(t)$ into seven non-intersecting compartments of susceptible individuals $S(t)$, fully vaccinated individuals $V(t)$, exposed individuals $E(t)$, asymptomatic infectious individuals $A(t)$, symptomatic infectious individuals $I(t)$, hospitalized individuals $H(t)$, and recovered individuals $R(t)$. The total population size is given by

$$N(t) = S(t) + V(t) + E(t) + A(t) + I(t) + H(t) + R(t).$$

The variable $x(t)$ denotes the proportion of individuals who play strategy one; that is, they vaccinate with each booster on time to keep their immunity up to date. Variable $K(t)$ denotes the capital, such as a country's gross domestic product. Table 1 lists the variables and their descriptions. The epidemic component of the model we will consider is closest to a model considered by Diagne et al. [30];

however, we also include game-theoretic and economic components. The following system gives the model:

$$\begin{aligned}
\frac{dS}{dt} &= \Lambda(1-x) - \frac{(\beta_I I + \beta_A A + \beta_H H)S}{N} - (\mu + \psi x)S + \omega_R R + \omega_V V \\
\frac{dV}{dt} &= \Lambda x + \psi x S - (1-\epsilon)\frac{(\beta_I I + \beta_A A + \beta_H H)V}{N} - (\mu + \omega_V)V \\
\frac{dE}{dt} &= \frac{(\beta_I I + \beta_A A + \beta_H H)S}{N} + (1-\epsilon)\frac{(\beta_I I + \beta_A A + \beta_H H)V}{N} - (\kappa + \mu)E \\
\frac{dA}{dt} &= (1-\rho)\kappa E - (\gamma_A + \mu)A \\
\frac{dI}{dt} &= \rho\kappa E - (\alpha + \gamma_I + \nu_i + \mu)I \\
\frac{dH}{dt} &= \alpha I - (\gamma_H + \nu_h + \mu)H \\
\frac{dR}{dt} &= \gamma_A A + \gamma_I I + \gamma_H H - (\mu + \omega_R)R \\
\frac{dx}{dt} &= x(1-x)(\delta_0 x - r_S + cH - \delta_0(1-x) + \eta K) \\
\frac{dK}{dt} &= sK^{\sigma}(N - \varepsilon_0 I - H)^{1-\sigma} - (d + \xi_h H)\,K.
\end{aligned} \tag{2.1}$$

In this model, Λ is the recruitment rate of individuals in the population, $\beta_I, \beta_A, \beta_H$ are the transmission rates from infective individuals I, asymptomatic individuals A, and hospitalized individuals H, respectively, μ is the natural death rate, ψ is the vaccination rate, ω_R, ω_V is the immunity waning rate for recovered R and vaccinated V individuals, respectively.

Table 1. Descriptions of the model variables representing the epidemiological, behavioral, and economic states in the system.

Variable	Description
S	Susceptible
V	Vaccinated
E	Exposed
A	Asymptomatic
I	Infected
H	Hospitalized
R	Recovered
x	Fraction completely immunized
K	Capital / GDP
N	Total population size

Parameter ϵ gives the vaccine efficacy, $1/\kappa$ is the length of the exposed period, ρ is the fraction of individuals who exhibit symptoms of COVID-19, α is the hospitalization rate, γ_I, γ_A, γ_H are the recovery rates for symptomatic infectious, asymptomatic infectious, and hospitalized individuals, respectively. δ_0 is the strength of social norms to follow health directives, r_S is the cost of vaccination,

c is a proportionality constant of the impact of number hospitalized on the decision to get vaccinated, η is proportionality constant of the economic impact on the decision to get vaccinated, s is the capital accumulation rate, d is the capital depreciation rate, and σ is the Elasticity of the output concerning capital. For a more detailed derivation of the game-theoretic-economic part, we refer to [28].

The growth of capital (K) follows a production function $sK^{\sigma}(N - \varepsilon_0 I - H)^{1-\sigma}$ that demonstrates a diminished labor efficiency due to both infected (I) and hospitalized (H) individuals. The capital K undergoes depreciation because of intrinsic decay rates (d) along with healthcare-related burdens ($\xi_h H$). K functions as both a determinant of vaccination behavior (ηK) and an outcome of disease prevalence, which leads to bidirectional coupling. Economic output declines during outbreaks because labor resources become scarce and equipment wears out more quickly, but improved economic capacity ($K \uparrow$) helps boost vaccination rates, which reduce disease transmission. The relationship between public health measures and economic stability underscores the need to harmonize these factors to ensure sustainable results. A list of parameters and their meanings is given in Table 2. The flowchart of the model is shown in Figure 1.

Table 2. Descriptions of model parameters used in the epidemiological–behavioral–economic framework.

Parameter	Description
Λ	Recruitment rate
β_I	Transmission rate from symptomatic infectious individuals
β_A	Transmission rate from asymptomatic infectious individuals
β_H	Transmission rate from hospitalized individuals
γ_I	Recovery rate of symptomatic infectious individuals
γ_A	Recovery rate of asymptomatic infectious individuals
γ_H	Recovery rate of hospitalized infectious individuals
ψ	Vaccination rate
ϵ	Vaccine efficacy
μ	Natural death rate
ω_R	Immunity waning while recovered
ω_V	Immunity waning while vaccinated
$1/\kappa$	Duration of exposed period
ν	Disease-induced death rate
α	Hospitalization rate
ρ	Proportion symptomatic individuals
η	Proportionality constant of the economic impact of the decision to get vaccinated
δ_0	Rate of individuals following the social norms
r_S	Cost of vaccination rate
d	Capital depreciation rate
c	Proportionality constant of hospitalizations impacting vaccinations
σ	Elasticity of the output concerning capital
ε_0	Labor efficiency reduction due to infected and hospitalized individuals

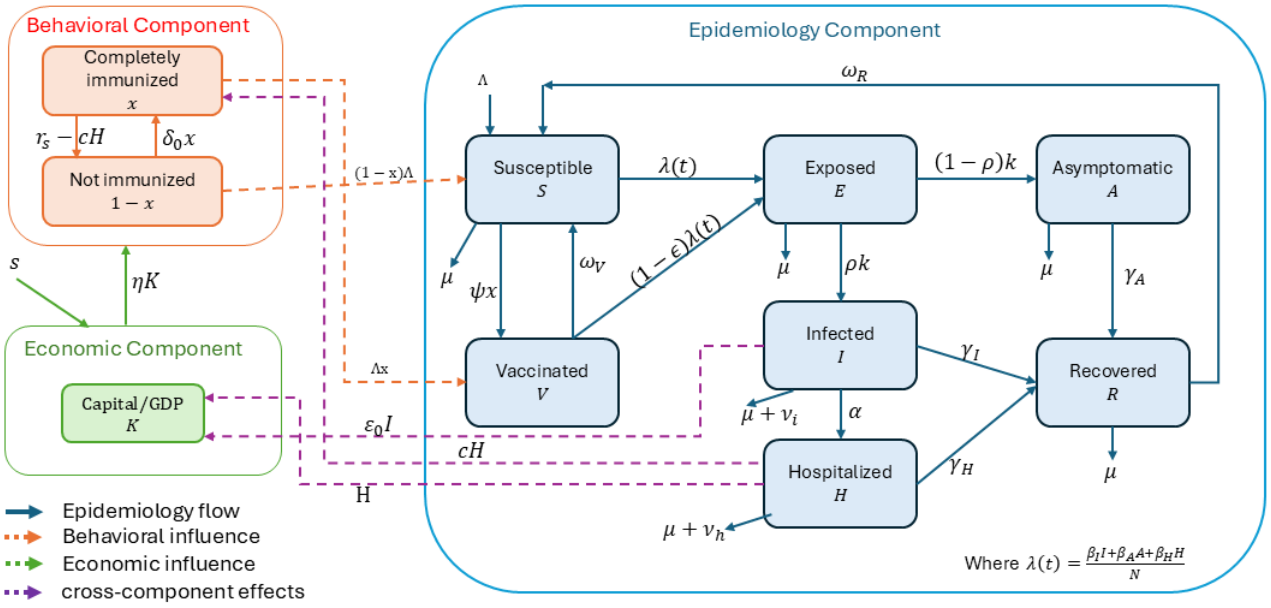

Figure 1. Compartmental model of COVID-19 vaccination dynamics with interacting components. The epidemiological component (blue) tracks population flow between disease states (S, V, E, A, I, H, R). The behavioral component (orange) models vaccination decisions (x vs $1 - x$), with red arrows showing how these choices affect disease spread. The economic component (green) represents capital (K) affected by labor availability. Purple dotted arrows show feedback mechanisms: hospitalizations influence vaccination decisions, while infections impact economic productivity. This bidirectional coupling demonstrates how disease outbreaks reduce economic output, while improved economic conditions can increase vaccination rates.

We adopt a continuous-time neoclassical growth framework based on the Solow-Swan model [31, 32], which describes capital accumulation driven by savings and depreciation. The capital stock $K(t)$ evolves as $\frac{dK}{dt} = sY(t) - dK(t)$, where $s > 0$ is the savings or capital stock accumulation rate and $d > 0$ is the depreciation rate. Assuming unit labor-augmenting technology, economic output ($Y(t)$) follows the Cobb-Douglas production function [33] $Y(t) = K(t)^{\sigma}(L(t))^{1-\sigma}$, with $\sigma \in (0, 1)$ denoting the capital share of output and $L(t)$ the labor force. Assuming diminishing returns to capital, the marginal productivity of capital declines as it accumulates.

At equilibrium, where $\frac{dK}{dt} = 0$, substituting the production function into (2.1) yields the equilibrium capital level: $K^* = 0$ or $K^* = \left(\frac{s}{d}\right)^{\frac{1}{1-\sigma}}$. Stability is assessed by examining the derivative of the accumulation function $f(K) = sK^{\sigma} - dK$. The slope at equilibrium is $\frac{df(K^*)}{dK} = d(\sigma - 1)$, which is negative under the standard condition $\sigma < 1$, confirming local asymptotic stability. The zero-capital equilibrium $K = 0$ is unstable due to unbounded marginal productivity as capital approaches zero. Thus, the model predicts convergence to a unique, stable equilibrium, where capital investment balances depreciation and diminishing returns. In the early stages of capital scarcity, high marginal

returns generate instability, but the system naturally stabilizes over time.

This framework component is linked to the rest of the framework through the production function and capital loss. Specifically, labor input is assumed proportional to the productive population, modifying the production function to $Y = K^{\sigma}(N - \varepsilon_0 I - H)^{1-\sigma}$, where $\varepsilon_0 \in [0, 1]$ accounts for reduced productivity among the infected. This form reflects reduced labor efficiency due to illness and hospitalization. Additionally, the capital loss term incorporates both intrinsic capital decay and health-related burdens, modifying the capital dynamics to include: $\frac{dK}{dt} = sY - (d + \xi_h H)K$, ξ_h captures the economic cost of hospitalization. Capital K determines economic output and influences vaccination behavior through a coupling term ηK, creating feedback between economic and epidemiological systems. During outbreaks, economic output declines as labor becomes scarce and capital deteriorates more rapidly. Conversely, improved economic capacity enhances vaccination uptake, reducing disease spread. This bidirectional interaction underscores the importance of integrating economic dynamics with health behavior models.

To formulate the model, we make several simplifying assumptions:

1) We assume a homogeneously mixing population and exponentially distributed times in epidemic classes, enabling us to formulate a simple ODE model. More realistically distributed times in epidemic classes require partial differential equations or more complex ODEs [34, 35].

2) We assume individuals in the vaccinated class are fully vaccinated and up-to-date on the boosters. According to the CDC, as of December 2022, this was valid for 27% of the US population [36]. Even if individuals are fully vaccinated and boosted, we assume their immunity wanes [37], and we assume they return to the susceptible class where they can be vaccinated again. Further, the vaccine is imperfect, leading to infection of vaccinated individuals at a reduced force of infection [38].

3) Upon infection, infected individuals enter a latent class, after which they develop symptoms and become infectious, or they become infectious and do not have symptoms. In reality, infected individuals are infective a couple of days before developing symptoms, and some researchers have modeled that by incorporating pre-symptomatic class [39] or by assuming that exposed individuals are infectious [40]. Still, we neglect it since this period lasts only a few days.

4) We assume that people are motivated to get vaccinated from reports of hospitalized individuals only, since the hospitalized individuals are a more reliable measure of the outbreak's severity. For the derivation of the game-theoretic and economic components of the model and their associated assumptions, we refer to [28].

The literature abounds with COVID-19 mathematical models, most of which are more complex than the one we present here. Our model's novelty incorporates a game-theoretic and an economic component, which are integrated into the model in the simplest possible way. Our goal is to study the model analytically and numerically and to understand the interplay between COVID-19, the vaccine decisions made by individuals, and the economy.

3. Mathematical analysis of the model

In this section, we provide a detailed mathematical analysis of the equilibrium solutions of the given model. The analysis identifies possible disease-free equilibria (DFE) by solving the system of equations and examines the conditions under which these equilibria exist.

3.1. Disease-free equilibrium solutions

This model has several disease-free equilibrium solutions. To find the disease-free equilibrium solutions, we set the time derivatives of the system to zero and the disease variables equal to zero, reducing the problem to solving the following algebraic equations:

$$0 = \Lambda(1-x) - (\mu + \psi x)S + \omega_V V, \tag{3.1}$$
$$0 = \Lambda x + \psi x S - (\mu + \omega_V)V, \tag{3.2}$$
$$0 = x(1-x)(\delta_0 x - r_S - \delta_0(1-x) + \eta K), \tag{3.3}$$
$$0 = sK^{\sigma}N^{1-\sigma} - dK. \tag{3.4}$$

Solution of Eq (3.4) The fourth equation, (3.4), determines the value of K. Assuming $\sigma = 1/2$, the solutions are $K = 0$ or

$$K = \left(\frac{s}{d}\right)^2 N.$$

These two possibilities divide the analysis into cases where $K = 0$ (no resources) or $K > 0$ (presence of resources).

Solution of Eq (3.3) The third equation, (3.3), determines the value of x. It admits three possible solutions: $x = 0$, $x = 1$, or a solution x^* that satisfies $0 < x^* < 1$. For $0 < x < 1$, the solution x^* is given by:

$$x^* = \frac{r_S + \delta_0}{2\delta_0}.$$

$x^* \in (0, 1)$ if and only if $r_S < \delta_0$.

3.2. Case analysis of disease-free equilibria

Combining the solutions of (3.4) and (3.3), we derive six cases, as outlined below.

1) **Case 1:** $K = 0$ **and** $x = 0$

Substituting into Eqs (3.1) and (3.2), the system becomes:

$$\Lambda - \mu S + \omega_V V = 0,$$
$$-\mu V - \omega_V V = 0.$$

These equations imply $S = \frac{\Lambda}{\mu}$ and $V = 0$. Thus, the first disease-free equilibrium is:

$$E_0 = \left(\frac{\Lambda}{\mu}, 0, 0, 0, 0, 0, 0, 0, 0\right).$$

2) **Case 2:** $K = 0$ **and** $x = 1$

For $x = 1$, Eqs (3.1) and (3.2) reduce to:

$$\begin{aligned} -(\mu + \psi)S + \omega_V V &= 0, \\ \Lambda + \psi S - (\mu + \omega_V)V &= 0. \end{aligned}$$

Solving these, we find:

$$\begin{aligned} V &= \frac{\Lambda(\psi + \mu)}{\mu(\mu + \psi + \omega_V)} := V_1^*, \\ S &= \frac{\Lambda\omega_V}{\mu(\mu + \psi + \omega_V)} := S_1^*. \end{aligned}$$

Thus, the second disease-free equilibrium is:

$$E_1 = (S_1^*, V_1^*, 0, 0, 0, 0, 0, 1, 0).$$

3) **Case 3:** $K = 0$ **and** $x = x^*$

For $x^* = \frac{r_S + \delta_0}{2\delta_0}$, Eqs (3.1) and (3.2) yield:

$$\begin{aligned} S_2^* &= \frac{\Lambda}{\mu} \cdot \frac{\mu(1 - x^*) + \omega_V}{\mu + \psi x^* + \omega_V}, \\ V_2^* &= \frac{\Lambda x^*}{\mu} \cdot \frac{\mu + \omega_V}{\mu + \psi x^* + \omega_V}. \end{aligned}$$

The third disease-free equilibrium is:

$$E_2 = (S_2^*, V_2^*, 0, 0, 0, 0, 0, x^*, 0).$$

4) **Case 4:** $K = K_0^*$ **and** $x = 0$

Here, substituting $x = 0$ into the equations for the disease process yields:

$$E_3 = \left(\frac{\Lambda}{\mu}, 0, 0, 0, 0, 0, 0, 0, K_0^*\right).$$

5) **Case 5:** $K = K_0^*$ **and** $x = 1$

For $x = 1$, the equilibrium becomes:

$$E_4 = (S_2^*, V_2^*, 0, 0, 0, 0, 0, 1, K_0^*),$$

where S_2^* and $V_@^*$ are as defined in Case 3.

6) **Case 6:** $K = K_0^*$ **and** $x = x_0^*$

If x_0^* is a solution of:

$$2\delta_0 x - r_S - \delta_0 + \eta K_0^* = 0,$$

Then:

$$x_0^* = \frac{r_S + \delta_0 - \eta K_0^*}{2\delta_0},$$

provided $0 < x_0^* < 1$. This condition holds if and only if:

$$\frac{r_S - \delta_0}{\eta} < K_0^* < \frac{r_S + \delta_0}{\eta}.$$

The final disease-free equilibrium is:

$$E_5 = (S_3^*, V_3^*, 0, 0, 0, 0, 0, x_0^*, K_0^*),$$

where S_3^*, V_3^* are obtained from $S_@^*, V_2^*$ in which the value of $x^* = 1$ has been replaced by x_2^*.

The six cases outlined above represent all possible disease-free equilibria for the model under different assumptions about K and x. Each equilibrium describes a biologically meaningful scenario that captures distinct states of the system in the absence of disease progression.

3.3. Stability of DFE

The disease-free equilibrium (DFE) stability is analyzed using the Jacobian matrix and evaluated at each DFE. The Jacobian matrix is given by

$$J = \begin{bmatrix} -(\mu+\psi x^*) & \omega_V & 0 & -\frac{\beta_A S^*}{S^*+V^*} & -\frac{\beta_I S^*}{S^*+V^*} & -\frac{\beta_H S^*}{S^*+V^*} & \omega_R & -\Lambda-\psi S^* & 0 \\ \psi x^* & -(\mu+\omega_V) & J_{24} & J_{25} & J_{26} & 0 & \Lambda+\psi S^* & 0 & \\ 0 & 0 & J_{33} & J_{34} & J_{35} & J_{36} & J_{37} & 0 & 0 \\ 0 & 0 & k(1-\rho) & -\gamma_A-\mu & 0 & 0 & 0 & 0 & 0 \\ 0 & 0 & k\rho & 0 & J_{55} & 0 & 0 & 0 & 0 \\ 0 & 0 & 0 & 0 & \alpha & J_{66} & 0 & 0 & 0 \\ 0 & 0 & 0 & \gamma_A & \gamma_I & \gamma_H & -\mu-\omega_R & 0 & 0 \\ 0 & 0 & 0 & 0 & 0 & cx(1-x) & 0 & J_{88} & \eta x(1-x) \\ J_{91} & J_{92} & J_{93} & J_{94} & J_{95} & -K\xi_h & J_{97} & 0 & J_{99} \end{bmatrix},$$

where,

$$J_{24} = -\frac{(1-\epsilon)\beta_A V^*}{S^*+V^*}, \quad J_{25} = -\frac{(1-\epsilon)\beta_I V^*}{S^*+V^*}, \quad J_{26} = -\frac{(1-\epsilon)\beta_H V^*}{S^*+V^*},$$

$$J_{33} = -(k+\mu), \quad J_{34} = \frac{\beta_A S^*}{N^*} + (1-\epsilon)\frac{\beta_A V^*}{N^*}, \quad J_{35} = \frac{\beta_I S^*}{N^*} + (1-\epsilon)\frac{\beta_I V^*}{N^*}, \quad J_{36} = \frac{\beta_H S^*}{N^*} + (1-\epsilon)\frac{\beta_H V^*}{N^*},$$

$$J_{88} = (1-2x^8)(\delta_0 x^* - r_S - \delta_0(1-x^*) + \eta K^*) + 2\delta_0 x^*(1-x^*),$$

$$J_{9j} = (1-\sigma)K^\sigma s(S^*+V^*)^{-\sigma}, j = 1,2,3,4,7, \quad J_{95} = (1-\sigma)K^\sigma s(S^*+V^*)^{-\sigma}(1-\epsilon_0),$$

$$J_{94} = K^\sigma s(S^*+V^*)^{1-\sigma}, \quad J_{99} = s\sigma K^{\sigma-1}N^{1-\sigma} - d,$$

$$J_{55} = -\alpha - \gamma_I - \mu - \nu_i, \quad J_{66} = -\gamma_H - \mu - \nu_h,$$

The eigenvalues of the Jacobian matrix determine the stability of the equilibrium points. Below, we analyze the stability of each equilibrium point in detail.

Now, we discuss the stability of all six disease-free equilibrium points above.

1) **Equilibrium E_0:**

Equilibrium E_0 is unstable if

$$s\sigma K^{\sigma-1}N^{1-\sigma} - d > 0 \quad \text{as} \quad K \to 0.$$

This inequality implies that E_0 is inherently unstable, as the term $s\sigma K^{\sigma-1}N^{1-\sigma}$ dominates as $K \to 0$.

2) **Equilibrium E_1:**

By an analogous argument to E_0, the equilibrium E_1 is also unstable under the same conditions.

3) **Equilibrium E_2:**

Similar reasoning indicates that E_2 is unstable. Thus, we conclude that all equilibria where $K = 0$ are unstable. This is sensible because no system can persist without resources.

4) **Equilibrium E_3:**

At E_3, one eigenvalue is given by:

$$s\sigma K_0^{*\sigma-1}N^{1-\sigma} - d.$$

Since $K_0^{*\sigma-1}N^{1-\sigma} = \frac{d}{s}$, it is not hard to see that at K_0^* this eigenvalue is always negative, since $\sigma < 1$. Some of the remaining eigenvalues are associated with the matrix:

$$J_1 = \begin{bmatrix} -(\mu + \psi x^*) & \omega_V \\ \omega_x & -(\mu + \omega_V) \end{bmatrix},$$

which has eigenvalues with negative real parts.

Additionally, another eigenvalue is given by:

$$\delta_0 x - r_S - \delta_0(1 - x) + \eta K_0^*|_{x=0} = -r_S - \delta_0 + \eta K_0^*.$$

Define the threshold:

$$r_1 = \frac{\eta K_0^*}{r_S + \delta_0}.$$

If $r_1 > 1$, E_3 is unstable. Assuming $r_1 < 1$, the remaining eigenvalues are determined by the characteristic equation of matrix J:

$$(\lambda + K + \mu)(\lambda + \gamma_A + \mu)(\lambda + \alpha + \gamma_I + \mu + \nu_i)(\lambda + \gamma_H + \mu + \nu_h) = 0.$$

The basic reproduction number $\mathcal{R}_1$ for E_3 is defined as:

$$\mathcal{R}_1 = \frac{\beta_A K(1-\rho)}{(K+\mu)(\gamma_A+\mu)} + \frac{\beta_I K\rho}{(K+\mu)(\alpha+\gamma_I+\mu+\nu_i)} + \frac{\beta_H \alpha\rho\kappa}{(K+\mu)(\alpha+\gamma_I+\mu+\nu_i)(\gamma_H+\mu+\nu_h)}.$$

If $\mathcal{R}_1 < 1$, E_3 can be locally asymptotically stable. Otherwise, it will be unstable. We summarize the results on E_3 stability in the following theorem.

Theorem 3.1. *Assume $r_1 < 1$ and $\mathcal{R}_1 < 1$. The equilibrium E_3 is locally asymptotically stable. If any of the three inequalities is reversed, E_3 is unstable.*

5) **Equilibrium E_4:**

At E_4, eigenvalues are determined by K_0^* and $x^* = 1$. Similar computations as before lead us to define:

$$r_2 = \frac{r_S}{\delta_0 + \eta K_0^*}.$$

Define also the disease reproduction number at $x^* = 1$ as $\mathcal{R}_2$, where:

$$\mathcal{R}_2 = \frac{k(1-\rho)(\beta_A(S_2^* + (1-\epsilon)V_2^*)}{(k+\mu 0(\gamma_A+\mu)(S_2^* + V_2^*)} + \frac{k\rho\beta_I(S_2^* + (1-\epsilon)V_2^*)}{(k+\mu)(\alpha+\gamma+I+\mu+\nu_i)(S_2^* + V_2^*)}$$

$$+\frac{k\rho\alpha\beta_H(S_2^* + (1-\epsilon)V_2^*)}{(k+\mu)(\alpha+\gamma+I+\mu+\nu_i)(\gamma_H+\mu+\nu_h)(S_2^* + V_2^*)},$$

we summarize the results on the stability of E_4 in the following theorem.

Theorem 3.2. *Assume $r_2 < 1$ and $\mathcal{R}_2$. Then E_4 is locally asymptotically stable. If any of these inequalities is reversed, E_4 is unstable.*

6) **Equilibrium E_5:**

The eigenvalues of J corresponding to E_5 are $\lambda_1 = -\mu, \lambda_2 = -(\mu + w_v + \psi x^*, \lambda_3 = 2\delta_0 x^*(1 - x^*), \lambda_4 = (\sigma - 1)d, \lambda_5 = -(\mu + w_v)$. The remaining eigenvalues of E_5 are the eigenvalues of the The characteristic equation is derived from a sub-matrix of the Jacobian J. Thus, the stability of E_5 is determined by the above eigenvalues and $\mathcal{R}_5$, where

$$\mathcal{R}_5 = \frac{k(1-\rho)(\beta_A(S_3^* + (1-\epsilon)V_3^*)}{(k+\mu 0(\gamma_A+\mu)(S_3^* + V_3^*)} + \frac{k\rho\beta_I(S_3^* + (1-\epsilon)V_3^*)}{(k+\mu)(\alpha+\gamma+I+\mu+\nu_i)(S_3^* + V_3^*)}$$

$$+\frac{k\rho\alpha\beta_H(S_3^* + (1-\epsilon)V_3^*)}{(k+\mu)(\alpha+\gamma+I+\mu+\nu_i)(\gamma_H+\mu+\nu_h)(S_3^* + V_3^*)},$$

if $\mathcal{R}_5 < 1$, E_5 would be locally asymptotically stable. If $\mathcal{R}_5 > 1$, E_5 would be unstable. However, eigenvalue $2\delta_0 x^*(1 - x^*)$ is always positive. Thus, E_5 is always unstable. We summarize the result on the stability of E_5 in the following theorem.

Theorem 3.3. *Equilibrium E_5 is always unstable.*

Stability analysis reveals that the equilibria E_0, E_1, E_2, and E_5 are inherently unstable for the parameter regimes considered. The equilibria E_3 and E_4 exhibit stability under specific threshold conditions related to r_1, r_2, $\mathcal{R}_1$, and $\mathcal{R}_2$. The reproduction numbers $\mathcal{R}_1$ and $\mathcal{R}_2$ provide critical information on the system's dynamics and the effectiveness of control measures. The instability of E_5 is unusual, but it follows from our assumptions on the fitness of the two strategies.

3.4. Existence of endemic equilibrium

To determine the presence of an endemic equilibrium for the system (2.1), we argue the existence of an endemic equilibrium by solving the following system of equations:

$$
\begin{aligned}
0 &= \Lambda(1-x) - \frac{(\beta_I I + \beta_A A + \beta_H H)S}{N} - (\mu + \psi x)S + \omega_R R + \omega_V V,\\
0 &= \Lambda x + \psi x S - (1-\epsilon)\frac{(\beta_I I + \beta_A A + \beta_H H)V}{N} - (\mu + \omega_V)V,\\
0 &= \frac{(\beta_I I + \beta_A A + \beta_H H)S}{N} + (1-\epsilon)\frac{(\beta_I I + \beta_A A + \beta_H H)V}{N} - (\kappa + \mu)E,\\
0 &= (1-\rho)\kappa E - (\gamma_A + \mu)A,\\
0 &= \rho\kappa E - (\alpha + \gamma_I + \nu_i + \mu)I,\\
0 &= \alpha I - (\gamma_H + \nu_h + \mu)H,\\
0 &= \gamma_A A + \gamma_I I + \gamma_H H - (\mu + \omega_R)R,\\
0 &= x(1-x)(\delta_0 x - r_S + cH - \delta_0(1-x) + \eta K),\\
0 &= sAK^{\sigma}(N - \varepsilon_0 I - H)^{1-\sigma} - (d + \xi_h H)\,K,\\
0 &= \Lambda - \mu N - \nu_i I - \nu_h H,
\end{aligned}
\tag{3.5}
$$

where,

$$N = \frac{\Lambda - \nu_i I - \nu_h H}{\mu} = \frac{\Lambda}{\mu} - \frac{\nu_i I}{\mu} - \frac{\nu_h H}{\mu}.$$

Substituting this into the ninth equation, we obtain:

$$0 = sK^{\sigma}\left(\frac{\Lambda}{\mu} - \left(\frac{\nu_i}{\mu} + \varepsilon_0\right)I - \left(1 + \frac{\nu_h}{\mu}\right)H\right)^{1-\sigma} - (d + \xi_h H)\,K.$$

Now, let $Q = \frac{\beta_I I + \beta_A A + \beta_H H}{N}$, which represents the force of infection. Using this substitution, we compute the equilibrium values of the other compartments:

$$
\begin{aligned}
E &= \frac{Q(S + (1-\epsilon)V)}{k + \mu},\\
I &= \frac{\rho k E}{(\alpha + \gamma_I + \nu_i + \mu)} = \frac{\rho k}{(\alpha + \gamma_I + \nu_i + \mu)}\frac{Q(S + (1-\epsilon)V)}{(k + \mu)} = iQ(S + (1-\epsilon)V,\\
H &= \frac{\alpha}{(\gamma_H + \nu_h + \mu)}\frac{\rho k}{(\alpha + \gamma_I + \nu_i + \mu)}\frac{Q(S + (1-\epsilon)V)}{(k + \mu)} = hQ(S + (1-\epsilon)V),\\
A &= \frac{(1-\rho)k}{(\gamma_A + \mu)}\frac{Q(S + (1-\epsilon)V)}{(k + \mu)} = aQ(S + (1-\epsilon)V),\\
R &= \frac{\gamma_A}{(\mu + \Omega_R)}\frac{(1-\rho)k}{(\gamma_A + \mu)}\frac{Q(S + (1-\epsilon)V)}{(k + \mu)} = pQ(S + (1-\epsilon)V).
\end{aligned}
$$

To simplify, let us rewrite the equations for S and V from the first two equations of the system:

$$\Lambda(1-x) - QS - (\mu + \psi x)S + \omega_R pQ(S + (1-\epsilon)V) + \omega_V V = 0, \tag{3.6}$$

$$\Lambda x + \psi x S - (1-\epsilon)QV - (\mu + \omega_V)V = 0. \tag{3.7}$$

Now we solve systems (3.6) and (3.7), and get

$$S = \frac{\Lambda(1-x)[(1-\epsilon)Q+\mu+\omega_V]+\Lambda x[(1-\epsilon)pQ\omega_R+\omega_V]}{[Q(1-\omega_R p)+\mu+\psi x][Q(1-\epsilon)+\mu+\omega_V]-[(1-\epsilon)Qp\omega_R+\omega_V]\psi x},$$

$$V = \frac{\Lambda(1-x)\psi x+\Lambda x[Q(1-p\omega_R)+\mu+\psi x]}{[Q(1-\omega_R p)+\mu+\psi x][Q(1-\epsilon)+\mu+\omega_V]-[(1-\epsilon)Qp\omega_R+\omega_V]\psi x}.$$

Let

$$S = f(Q,x) \quad \text{and} \quad V = g(Q,x).$$

The equation for N is $\Lambda-\mu N-\nu_i I-\nu_h H=0$ which gives

$$N = \frac{\Lambda}{\mu}-\frac{\nu_i}{\mu}I-\frac{\nu_h}{\mu}H = \frac{\Lambda}{\mu}-\frac{\nu_i}{\mu}iQ(S+(1-\epsilon)V)-\frac{\nu_h}{\mu}hQ(S+(1-\epsilon)V)$$

and

$$\begin{aligned} Q &= \frac{\beta_I I+\beta_A A+\beta_H H}{N} \\ &= \frac{\beta_I iQ[f(Q,x)+(1-\epsilon)g(Q,x)]+\beta_A aQ[f(Q,x)+(1-\epsilon)g(Q,x)]+\beta_H hQ[f(Q,x)+(1-\epsilon)g(Q,x)]}{\frac{\Lambda}{\mu}-\left(\frac{\nu_i}{\mu}i+\frac{\nu_h}{\mu}h\right)Q\,(f(Q,x)+(1-\epsilon)g(Q,x))}. \end{aligned} \tag{3.8}$$

Thus, the equation for Q is

$$\frac{(\beta_I i+\beta_A a+\beta_H h)(f(Q,x)+(1-\epsilon)g(Q,x))}{\frac{\Lambda}{\mu}-(\frac{\nu_i i+\nu_h h}{\mu})Q(f(Q,x)+(1-\epsilon)g(Q,x))}=1. \tag{3.9}$$

Case 1: $x=0$ (no one is a vaccinator)

$$S = \frac{\Lambda((1-\epsilon)Q+\mu+\omega_V}{[(1-\omega_R p)Q+\mu][(1-\epsilon)Q+\mu+\omega_V]} = \frac{\Lambda}{(1-\omega_R p)Q+\mu} = f(Q),$$

$V=0$ implies $g(Q)=0$ and Eq (3.9) of Q becomes

$$\frac{(\beta_I i+\beta_A a+\beta_H h)\Lambda}{\frac{\Lambda}{\mu}((1-\omega_R p)Q+\mu)-(\frac{\nu_i i+\nu_h h}{\mu})\Lambda Q}=1. \tag{3.10}$$

We note that in the above, the denominator of f in the numerator and denominator of the left-hand side of (3.10) cancels. Considering the denominator of (3.10), we show it remains positive for all Q.

$$\begin{aligned} 1-\omega_R p-\nu_i i-\nu_h h &= 1-\frac{\omega_R}{\mu+\omega_R}\frac{(1-\rho)k}{\mu+k}\frac{\gamma_A}{\mu+\gamma_A}-\frac{\nu_i}{\alpha+\gamma_I+\mu+\nu_i}\frac{\rho k}{\mu+k} \\ &\quad -\frac{\nu_h}{\gamma_H+\mu+\nu_h}\frac{\rho k}{\mu+k}\frac{\alpha}{\alpha+\gamma_I+\nu_i+k} \\ &\geq 1-\frac{\omega_R}{\mu+\omega_R}\frac{(1-\rho)k}{\mu+k}\frac{\gamma_A}{\mu+\gamma_A}-\frac{\rho k}{\mu+k}\frac{\nu_i+\alpha}{\alpha+\gamma_I+\mu+\nu_i} \\ &\geq 1-\frac{(1-\rho)k}{\mu+k}-\frac{\rho k}{\mu+k}=1-\frac{k}{k+\mu}=\frac{\mu}{k+\mu}>0 \end{aligned}$$

Thus, the denominator is always positive. Therefore, the left-hand side of (3.10) is a decreasing function of Q. Thus, if

$$R_6 = \beta_I i + \beta_A a + \beta_H h > 1. \tag{3.11}$$

then there is a unique solution Q, which gives a unique endemic equilibrium.

Theorem 3.4. *If* (3.11) *holds, the system has a unique endemic equilibrium with* $x = 0$.

Case 2: When $x = 1$, we get

$$S = \frac{\Lambda[(1-\epsilon)\omega_R pQ + \omega_V]}{[(1-\omega_R p)Q + \mu + \psi][(1-\epsilon)Q + \mu + \omega_V] - [(1-\epsilon)\omega_R pQ + \omega_V]\psi} = f(Q), \tag{3.12}$$

$$V = \frac{\Lambda[Q(1-\omega_R p) + \mu + \psi]}{[(1-\omega_R p)Q + \mu + \psi][(1-\epsilon)Q + \mu + \omega_V] - [(1-\epsilon)\omega_R pQ + \omega_V]\psi} = g(Q). \tag{3.13}$$

Now, we evaluate the LHS of (3.9) at $Q = 0$, and we get

$$S_{Q=0} = \frac{\Lambda\omega_V}{(\mu+\psi)(\mu+\omega_V\psi) - \omega_V\psi} = f(0),$$

$$V_{Q=0} = \frac{\Lambda(\mu+\psi)}{[(\mu+\psi)(\mu+\omega_V) - \omega_V\psi} = g(0),$$

$$R_7 = \frac{(\beta_I i + \beta_A a + \beta_H h)[f(0) + (1-\epsilon)g(0)]}{\Lambda/\mu}.$$

The denominator in the expressions for S and V above is

$$denom = [(1-\omega_R p)Q + \mu]\,[(1-\epsilon)Q + \mu + \omega_V] + \psi(1-\epsilon)Q(1-\omega_R p) + \psi\mu.$$

Thus, the denominator is an increasing function of Q. In the expressions for S and V above, the denominator is quadratic in Q, and the numerator is linear in Q. Thus, $f(Q) \to 0$ and $g(Q) \to 0$, as $Q \to \infty$.

Also,

$$Qf(Q) \to \frac{\Lambda(1-\epsilon)\omega_R p}{(1-\omega_R p)(1-\epsilon)} = \frac{\Lambda\omega_R p}{1-\omega_R p} \quad \text{as } Q \to \infty,$$

$$Qg(Q) \to \frac{\Lambda(1-\omega_R p)}{(1-\omega_R p)(1-\epsilon)} = \frac{\Lambda}{1-\epsilon} \quad \text{as } Q \to \infty.$$

Thus, as $Q \to \infty$, the LHS of (3.9) tends to

$$\frac{(\beta_I i + \beta_A a + \beta_H h)\cdot 0}{\frac{\Lambda}{\mu} - \frac{\Lambda}{\mu}(\nu_i i + \nu_h h)\left(\frac{\omega_R p}{1-\omega_R p} + 1\right)}.$$

Consider the denominator of the expression above:

$$\frac{\Lambda}{\mu}\left[1-(\nu_i i+\nu_h h)\left(\frac{\omega_R p}{1-\omega_R p}+1\right)\right]$$

$$=\frac{\Lambda}{\mu}\left[1-\left(\frac{\nu_i}{\alpha+\gamma_I+\nu_i+\mu}-\frac{\rho k}{k+\mu}+\frac{\nu_h}{\nu_h+\gamma_H+\mu}\cdot\frac{\rho k}{k+\mu}\cdot\frac{\alpha}{\alpha+\gamma_I+\nu_i+\mu}\right)\cdot\left(\frac{\omega_R p}{1-\omega_R p}+1\right)\right].$$

The expression in the second parenthesis can be simplified as follows:

$$\frac{\omega_R p+1-\omega_R p}{1-\omega_R p}=\frac{1}{1-\omega_R p}.$$

Thus,

$$1-\omega_R p-\frac{\nu_i}{\alpha i+\gamma_I+\nu_i+\mu}\frac{\rho k}{k+\mu}-\frac{\nu_h}{\nu_h+\gamma_I+\mu}\cdot\frac{\rho k}{k+\mu}\frac{\alpha}{\alpha+\gamma_I\nu_i+\mu}>0.$$

Therefore, $\lim_{Q\to\infty}$ of the LHS of (3.9) is zero. We obtain the following theorem.

Theorem 3.5. *If $R_7>1$, at least one solution with $x=1$ exists.*

Case 3: $0<x<1$ The equilibrial equations for K and x are given by:

$$sK^{\sigma}(N-\epsilon_0 I-H)^{1-\sigma}-(d+\xi_h H)K=0,$$

$$\delta_0 x-r_S+cH-\delta_0(1-x)+\eta k=0.$$

Solving the K equation. Let $\sigma=\frac{1}{2}$:

$$sK^{\frac{1}{2}}(N-\epsilon_0 I-H)^{\frac{1}{2}}=(d+\xi_h H)K.$$

Case 3A: $K=0$ The equation for x takes the form:

$$\delta_0 x-r_S+cH-\delta_0(1-x)=0,$$
$$2\delta_0 x+chQ[f(Q,x)+(1-\epsilon)g(Q,x)]=r_S+\delta_0,$$

where

$$S=\frac{\Lambda(1-x)[(1-\epsilon)Q+\mu+\omega_V]+\Lambda x[(1-\epsilon)\omega_R pQ+\omega_V]}{[(1-\omega_R p)Q+\mu+\psi x][(1-\epsilon)Q+\mu+\omega_V]-[(1-\epsilon)\omega_R pQ+\omega_V]\psi x}=:f(Q,x),$$

$$V=\frac{\Lambda(1-x)\psi x+\Lambda x[Q(1-\omega_R p)+\mu+\psi x]}{[(1-\omega_R p)Q+\mu+\psi x][(1-\epsilon)Q+\mu+\omega_V]-[(1-\epsilon)\omega_R pQ+\omega_V]\psi x}=:g(Q,x).$$

We need to decide whether $f(Q,x)+(1-\epsilon)g(Q,x)$ increases or decreases in x.

$$f+(1-\epsilon)g=\frac{\Lambda((1-\epsilon)Q+Q(1-\omega_R p)\epsilon x+\mu+\omega_V+\psi x)}{[(1-\omega_R p)Q+\mu+\psi x][(1-\epsilon)Q+\mu+\omega_V]-[(1-\epsilon)\omega_R pQ+\omega_V]\psi x}.$$

Taking the derivative with respect to x, we have

$$\frac{d}{dx}(f + (1-\epsilon)g)$$
$$= \frac{\epsilon Q(1-\omega_R p)(Q(1-\omega_R p)+\mu+\psi)((1-\epsilon Q+\mu+\omega_V)+(\epsilon Q(1-\omega_R p)+\psi)((1-\epsilon)Q(1-\omega_R p)+\mu)\psi x)}{(denom)^2}.$$

Consequently $f(Q,x)+(1-\epsilon)g(Q,x)$ is an increasing function of x. Thus, the left-hand side of

$$2\delta_0 x + chQ[f+(1-\epsilon)g] = r_S + \delta_0,$$

is an increasing function of x. At $x=0$ we want

$$chQ[f(Q,0)+(1-\epsilon)g(Q,0)] < r_S + \delta_0. \tag{3.14}$$

We note that $g(Q,0)=0$, and the above inequality follows if

$$\frac{chQ\Lambda}{((1-\omega_R p)Q+\mu)} < r_s + \delta_0.$$

Since the left-hand side of the above is an increasing function of Q, the inequality will be satisfied for all Q if we assume

$$\frac{ch\Lambda}{(1-\omega_R p)} < r_s + \delta_0. \tag{3.15}$$

Then, Eq (3.14) holds for any Q. At $x=1$ we want

$$chQ[f+(1-\epsilon)g] > r_S - \delta_0. \tag{3.16}$$

This inequality is clearly satisfied for all Q if $r_S < \delta_0$.

Hence, we have the following result:

Theorem 3.6. *Assume $r_S < \delta_0$ and*

$$chQ\frac{\Lambda((1-\epsilon)Q+\mu\omega_v)}{[(1-\omega_R)Q+\mu][(1-\epsilon)Q+\mu+\omega_V]} < r_S + \delta_0, \tag{3.17}$$

for all Q, that is, we assume inequality (3.15) *is satisfied. Then equation*

$$2\delta_0 x + chQ\{f(Q,x)+(1-\epsilon)g(Q,x)\} = r_S + \delta_0, \tag{3.18}$$

has a unique solution for $x \in (0,1)$.

From the above theorem, it follows that the solution defines $x = X(Q)$ for all Q. Changing x with $X(Q)$ in (3.8), we obtain an equation in Q. Consider (3.8) with $x = X(Q)$. Our goal is to show that the equation below has a solution,

$$\frac{(\beta_I i+\beta_A a+\beta_H h)(f(Q,X(Q))+(1-\epsilon)g(Q,X(Q)))}{\frac{\Lambda}{\mu}-(\frac{\nu_i i+\nu_h h}{\mu})Q(f(Q,X(Q))+(1-\epsilon)g(Q,X(Q)))} = 1. \tag{3.19}$$

We note that the denominator of the expression on the left-hand side above remains positive for all $Q, X \in [0,1]$. This result is due to Theorem 3.10 given below. Evaluating the left-hand side of (3.19) at $Q=0$, we get

$$R_8 = \frac{(\beta_I i + \beta_A a + \beta_H h)(f(0, x(0)) + (1-\epsilon)g(0, x(0)))}{\frac{\Lambda}{\mu}}.$$

For $Q = 0$ in (3.18) we get

$$2\delta_0 x = r_S + \delta_0 \Rightarrow x = \frac{r_S + \delta_0}{2\delta_0}.$$

Thus, $X(0) = \frac{r_S+\delta_0}{2\delta_0}$ and, consequently, $1 - X(0) = 1 - \frac{r_S+\delta_0}{2\delta_0} = \frac{\delta_0 - r_S}{2\delta_0}$. Hence, we have

$$\begin{aligned} f(0, X(0)) + (1-\epsilon)g(0, X(0)) = & \frac{\Lambda\left(\frac{\delta_0-r_S}{2\delta_0}\right)(\mu+\omega_V) + \Lambda\left(\frac{r_S+\delta_0}{2\delta_0}\right)\omega_V}{\left[\mu + \psi\left(\frac{r_S+\delta_0}{2\delta_0}\right)\right](\mu+\omega_V) - \omega_V\psi\left(\frac{r_S+\delta_0}{2\delta_0}\right)} \\ & + (1-\epsilon)\frac{\Lambda\left(\frac{\delta_0-r_S}{2\delta_0}\right)\psi\left(\frac{\delta_0+r_S}{2\delta_0}\right) + \Lambda\left(\frac{\delta_0-r_S}{2\delta_0}\right)\left(\mu + \psi\frac{\delta_0-r_S}{2\delta_0}\right)}{(\mu + \psi\frac{\delta_0-r_S}{2\delta_0})(\mu+\omega_V) - \omega_V\psi\frac{\delta_0-r_S}{2\delta_0}}. \end{aligned}$$

Next, we want to know what $X(\infty)$ is.

$$\begin{aligned} \lim_{Q\to\infty} Qf(Q, X) &= \frac{\Lambda(1-X)(1-\epsilon) + \Lambda X(1-\epsilon)\omega_R p}{(1-\epsilon)(1-\omega_R p)} \\ &= \frac{\Lambda(1-\epsilon)(1-X+X\omega_R p)}{(1-\epsilon)(1-\omega_R p)} = \frac{\Lambda(1-X(1-\omega_R p))}{(1-\omega_R p)}, \end{aligned}$$

and

$$\begin{aligned} \lim_{Q\to\infty} Qg(Q, X) &= \frac{\Lambda X(1-\omega_R p)}{(1-\epsilon)(1-\omega_R p)}, \\ Qf + (1-\epsilon)Qg &= \frac{\Lambda((1-\epsilon)(1-X(1-\omega_R p)) + (1-\epsilon)\Lambda X(1-\omega_R p)}{(1-\epsilon)(1-\omega_R p)} \\ &= \frac{\Lambda - \Lambda X(1-\omega_R p)) + \Lambda X(1-\omega_R p)}{(1-\omega_R p)} \\ &= \frac{\Lambda}{1-\omega_R p}, \end{aligned}$$

$$2\delta_0 X + ch\frac{\Lambda}{1-\omega_R p} = r_S + \delta_0,$$

$$X = \frac{r_S + \delta_0 - \frac{\Lambda ch}{1-\omega_R p}}{2\delta_0} = X(\infty).$$

We note that $X(\infty) \geq 0$, which follows from (3.15). Furthermore, since we assume that $r_S < \delta_0$, then $X(\infty) < 1$. Now, taking the limit as $Q \to \infty$ of LHS of (3.19) we get

$$\lim_{Q\to\infty} (f(Q, X(Q)) + (1-\epsilon)g(Q, X(Q))) = 0.$$

This discussion leads us to the following theorem.

Theorem 3.7. *Assume $r_S < \delta_0$ and the inequality* (3.15) *holds. If $R_8 > 1$, then* (3.19) *has at least one solution for Q, giving $0 < x^* < 1$.*

Remark: Q is capped as

$$Q = \frac{\beta_I I + \beta_A A + \beta_H H}{N} < \max\{\beta_I, \beta_A, \beta_H\}.$$

Case 3B: $K \neq 0$

$$sK^{1/2}(N - \epsilon_0 I - H)^{1/2} = (d + \xi_h H)K.$$

Canceling $K^{1/2}$, we obtain:

$$s(N - \epsilon_0 I - H)^{1/2} = (d + \xi_h H)K^{1/2}.$$

Solving for K, we have:

$$K^{1/2} = \frac{s(N - \epsilon_0 I - H)^{1/2}}{(d + \xi_h H)}.$$

Therefore, K can be expressed in terms of the number of infected and hospitalized individuals.

$$K = \frac{s^2(N - \epsilon_0 I - H)}{(d + \xi_h H)^2}.$$

From the equation for x, we obtain:

$$\delta_0 x - r_S + cH - \delta_0(1 - x) + \eta K = 0.$$

We are looking for a solution satisfying $0 < x < 1$. We replace K with its expression in I and H:

$$\delta_0 x - r_S + cH - \delta_0(1 - x) + \frac{\eta s^2(N - \epsilon_0 I - H)}{(d + \xi_h H)^2} = 0.$$

Consider the equation for N

$$0 = \Lambda - \mu N - \nu_i I - \nu_h H.$$

Solving for N in terms of I and H, we have:

$$N = \frac{\Lambda}{\mu} - \frac{\nu_i}{\mu} I - \frac{\nu_h}{\mu} H.$$

Thus, the equation for x becomes:

$$cH + \frac{\eta s^2(N - \epsilon_0 I - H)}{(d + \xi_h H)^2} = r_S + \delta_0 - 2\delta_0 x.$$

Replacing N with its expression in terms of I and H, we have:

$$cH + \frac{\eta s^2 \left(\frac{\Lambda}{\mu} - \frac{\nu_i}{\mu} I - \frac{\nu_h}{\mu} H - \epsilon_0 I - H\right)}{(d + \xi_h H)^2} = r_S + \delta_0 - 2\delta_0 x. \tag{3.20}$$

We rewrite the left-hand side of (3.20) in terms of I

$$c\alpha_1 I + \frac{\eta s^2\left(\frac{\Lambda}{\mu} - qI\right)}{(d+\xi_h\alpha_1 I)^2} = r_S + \delta_0 - 2\delta_0 x, \tag{3.21}$$

where $q = \frac{\nu_i}{\mu} + \frac{\nu_h}{\mu}\alpha_1 + \epsilon_0 + \alpha_1$ and $\alpha_1 = \frac{\alpha}{\gamma_H+\nu_h+\mu}$.

Theorem 3.8. *If*

$$c\alpha_1 d^3 - \eta s^2(dq + 2\frac{\Lambda}{\mu}\xi_h\alpha_1) > 0, \tag{3.22}$$

then the left hand side of (3.21) *is an increasing function of* I.

The proof of this theorem is omitted. If condition (3.22) is satisfied, then (3.20) is an increasing function of H and I. On the other hand, H and I are increasing functions of x. Thus, the left-hand side of (3.20) is an increasing function of x.

Assume

$$cH(0) + \frac{\eta s^2\left(\frac{\Lambda}{\mu} - \frac{\nu_i}{\mu}I(0) - \frac{\nu_h}{\mu}H(0) - \epsilon_0 I(0) - H(0)\right)}{(d+\xi_h H(0))^2} < r_S + \delta_0, \tag{3.23}$$

where $H(0), I(0)$ denote H and I evaluated at $x = 0$. Assume $r_S - \delta_0 < 0$. Then:

$$cH(1) + \frac{\eta S^2 A^2\left(\frac{\Lambda}{\mu} - \frac{\nu_i}{\mu}I(1) - \frac{\nu_h}{\mu}H(1) - \epsilon_0 I(1) - H(1)\right)}{(d+\xi_h H(1))^2} > r_S - \delta_0,$$

where $H(1), I(1)$ denote H and I evaluated at $x = 1$.

Then, (3.20) has a unique solution at $x \in (0,1)$. Denote this solution as follows:

$$x = X(Q).$$

Replacing x with $X(Q)$ in the expression for Q , we obtain the following equation for Q:

$$1 = \frac{(\beta_I i + \beta_A a + \beta_H h)(f(Q,X(Q)) + (1-\epsilon)g(Q,X(Q)))}{\frac{\Lambda}{\mu} - \left(\frac{\nu_i}{\mu}i + \frac{\nu_h}{\mu}h\right)Q\,(f(Q,X(Q)) + (1-\epsilon)g(Q,X(Q)))}. \tag{3.24}$$

Denote by

$$R_9 = \frac{(\beta_I i + \beta_A a + \beta_H h)(f(0,X(0)) + (1-\epsilon)g(0,X(0)))}{\frac{\Lambda}{\mu}}.$$

Consider (3.20) with $Q = 0$, which implies that $I = H = 0$. This gives

$$\frac{\eta s^2\frac{\Lambda}{\mu}}{d^2} = r_S + \delta_0 - 2\delta_0 x \Rightarrow x = \frac{r_S+\delta_0}{2\delta_0} - \frac{\eta s^2\frac{\Lambda}{\mu}}{2\delta_0 d^2} =: X(0).$$

We want $x \in (0,1)$. Thus, we define the number r_9 below. It is not hard to see that if $r_9 < 1$, then $X(0) \in (0,1)$.

Let

$$r_9 = \frac{c\alpha_1 i d^2\frac{\Lambda}{1-\omega_R p} + \eta s^2\frac{\Lambda}{\mu}}{d^2(r_S+\delta_0)}.$$

It can be shown that if $r_9 < 1$, then (3.23) holds for all Q. If, on the other hand, $R_9 > 1$, then the RHS of Eq (3.24) is greater than one. Next, as before, we have that

$$\lim_{Q\to\infty} Q(f(Q, X(Q)) + (1-\epsilon)g(Q, X(Q)) = \frac{\Lambda}{1-\omega_R p}.$$

Hence,

$$X(\infty) = \lim_{Q\to\infty} X(Q) = \frac{1}{2\delta_0}\left[r_S + \delta_0 - c\alpha_1 i\frac{\Lambda}{1-\omega_R p} - \frac{\eta s^2(\frac{\Lambda}{\mu} - qi\frac{\Lambda}{1-\omega_R p})}{(d + \xi_h\alpha_1 i\frac{\Lambda}{1-\omega_R p})^2}\right].$$

It is not hard to see that if $r_9 < 1$, $X(\infty) \in (0, 1)$. Because $Qf(Q, X(Q))$ and $Qg(Q, X(Q))$ have finite nonzero limits as Q goes to ∞, that means that

$$\lim_{Q\to\infty} f(Q, X(Q)) = 0 \qquad \textit{and} \qquad \lim_{Q\to\infty} g(Q, X(Q)) = 0.$$

Therefore, as $Q \to \infty$, the RHS of (3.24) goes to zero. Thus, as a function of Q, the RHS of (3.24) is larger than one for $Q = 0$ and goes to zero as $q \to \infty$. Hence, there must be a Q^* for which the RHS of (3.24) equals one. That Q gives an endemic equilibrium. We summarize these deliberations in the following theorem.

Theorem 3.9. *Assume $r_9 < 1$, $R_9 > 1$ and condition* (3.22) *hold. Then there is at least one endemic equilibrium with $0 < x_9^* < 1$ and $K_9^* > 0$, $E_9 = (S_9^*, V_9^*, E_9^*, A_9^*, I_9^*, H_9^*, R_9^*, x_9^*, K_9^*)$.*

For the above arguments to lead to Theorem 3.9, we need the denominator of (3.24) always to be positive for all Q and $x \in [0, 1]$. To demonstrate this result, we introduce the following theorem.

Theorem 3.10. *The denominator of* (3.24) *is positive for all Q and $x \in [0, 1]$.*

To see this theorem, we bound $f + (1-\epsilon)g$ from above. We rewrite the denominator as a sum:

$$\frac{1}{\Lambda}(f + (1-\epsilon)g) = \frac{(1-x)((1-\epsilon)Q + \mu + \omega_V + (1-\epsilon)\psi x) + x((1-\epsilon)Q + (1-\epsilon)\mu + \omega_V + (1-\epsilon)\psi x)}{((1-\omega_R p)Q + \mu)((1-\epsilon)Q + \mu + \omega_V) + \psi x((1-\epsilon)(1-\omega_R p)Q + \mu)}.$$

Rearranging the terms in the numerator, we have

$$\frac{1}{\Lambda}(f + (1-\epsilon)g) = \frac{((1-\epsilon)Q + \mu + \omega_V + (1-\epsilon)\psi x) - \epsilon x\mu}{denom}.$$

Neglecting the negative term in the numerator, we are going up. Thus, we have

$$\frac{1}{\Lambda}(f + (1-\epsilon)g) \le \frac{((1-\epsilon)Q + \mu + \omega_V + (1-\epsilon)\psi x)}{((1-\omega_R p)Q + \mu)((1-\epsilon)Q + \mu + \omega_V) + \psi x((1-\epsilon)(1-\omega_R p)Q + \mu)}.$$

By differentiation, it is not hard to show that the expression above is a decreasing function of ψx. Thus, if we set ψx to zero, we will obtain something larger. Therefore, we have

$$\frac{((1-\epsilon)Q + \mu + \omega_V}{((1-\omega_R p)Q + \mu)((1-\epsilon)Q + \mu + \omega_V)} \le \frac{1}{(1-\omega_R p)Q}.$$

Considering the denominator of (3.24) and using the estimate of $f + (1-\epsilon)g$ we have

$$denom \ge \frac{\Lambda}{\mu}\left(1 - (\nu_i i + \nu_h h)\frac{1}{(1-\omega_R p)}\right) = \frac{\Lambda}{\mu}\frac{1 - \omega_R p - \nu_i i - \nu_h h}{1-\omega_R p} > 0.$$

3.5. Control reproduction number

We define a control reproduction number, which will be used in the numerical simulations.

$$R_c = \frac{\kappa\left[B_2\rho(B_4\beta_I + \alpha\beta_H) + B_3B_4\beta_A(1-\rho)\right]}{B_1B_2B_3B_4}\left[\frac{S + (1-\varepsilon_V)\,V}{S+V}\right] = R_0\,(1-\varepsilon_V f_V)\,, \tag{3.25}$$

$B_1 = \kappa + \mu, B_2 = \gamma_A + \mu, B_3 = \alpha + \gamma_I + \nu_i + \mu, B_4 = \gamma_H + \nu_h + \mu$, $f_V = \frac{V}{S+V}$.

Herd immunity threshold: $f_v^* = \frac{1}{\varepsilon_V}\left(1 - \frac{1}{R_0}\right)$.

4. Model fitting to data and structural identifiability

4.1. Data fitting and parameter estimation

Using publicly available data, we calibrated the COVID-19 epidemiological model to daily case and death counts in the United States from November 20, 2021, to April 22, 2022. The model incorporates multiple compartments, including susceptible (S), vaccinated (V), exposed (E), asymptomatic (A), symptomatic (I), hospitalized (H), and recovered (R) individuals. Parameter estimation focused on key epidemiological rates, such as transmission and recovery, by minimizing the discrepancy between model predictions and observed data.

4.2. Data sources and preprocessing

Daily incidence and mortality data were initially obtained from the CDC website in March 2023. However, due to the discontinuation of COVID-19 case tracking, these data are no longer available on the CDC platform. Despite this, they remain essential for analyzing the pandemic's progression during that period. To mitigate potential biases from testing shortages and reporting delays, we estimated the initial effective population size, $N(0)$, held constant throughout parameter estimation. Additionally, we introduced a parameter ρ to account for asymptomatic and unreported cases, improving the model's ability to capture early-stage disease dynamics when testing capacity was limited. The dataset and accompanying code will be made available on GitHub upon request.

4.3. Parameter estimation approach

The estimated parameters include transmission, recovery, vaccination, death rates, and other model-specific parameters. They were estimated using a constrained optimization process. Due to the complexity and potential identifiability challenges inherent to the model, specific parameters were fixed based on values from the literature to ensure stable and accurate estimates.

4.4. Optimization process

The parameter estimation was formulated as a constrained optimization problem, where the objective function minimized the sum of squared differences between the observed data and the model's predictions. This was done while ensuring that the parameters remained within biologically plausible ranges. The optimization problem is defined as:

$$\hat{p} = \min_{p>0}\left(\frac{1}{n}\sum_{i=1}^{n}\left|\frac{y_1(t_i) - Y_{i1}}{\hat{Y}_1}\right|^2 + \frac{1}{m}\sum_{j=1}^{m}\left|\frac{y_2(t_j) - Y_{j2}}{\hat{Y}_2}\right|^2\right),$$

where p is the parameter vector, Y_{i1} and Y_{j2} are the observed daily cases and deaths, and $y_1(t_i)$ and $y_2(t_j)$ are the corresponding model-predicted values. The terms $\hat{Y}_1$ and $\hat{Y}_2$ are the average daily observed cases and deaths, respectively.

4.5. Best-fit parameter values

The parameter estimation process yielded the values presented in Table 3. These values represent the best-fit parameters that effectively capture the dynamics of COVID-19 during the specified period. The parameters provide a robust fit to the data, reflecting the underlying transmission and progression of the disease. Figure 2 illustrates the model's fit to the data.

Table 3. Best-fit parameter values for the COVID-19 model.

Parameter	Value	Unit	Reference
Λ	12000	# people/day	computed
μ	1/(365*77)	days^{-1}	[41]
β_I	2.331941756049400	days^{-1}	fitted
β_A	0.489195394362985	days^{-1}	fitted
β_H	2.808321751437552	days^{-1}	fitted
γ_I	0.999413086787279	days^{-1}	fitted
γ_A	0.431693071216958	days^{-1}	fitted
γ_H	0.142855222286123	days^{-1}	fitted
ψ	0.009179791490040	days^{-1}	fitted
ϵ	0.85	Dimensionless	[39]
ω_R	1/90 days^{-1}	days^{-1}	[30]
ω_V	1/120 days^{-1}	days^{-1}	[37]
$1/\kappa$	5	days^{-1}	[25]
ν_i	0.005905364597948	days^{-1}	fitted
ν_h	0.124008505776642	days^{-1}	fitted
α	1/5 days^{-1}	days^{-1}	[39]
ρ	0.168587872308369	Unitless	fitted
η	0.028370082249179	(days $\times$ dollars)$^{-1}$	fitted
δ_0	0.328196677991075	days^{-1}	fitted
r_S	1.921848796624883	days^{-1}	fitted
d	2.996338283133039	days^{-1}	fitted
c	1.948939475929112	(days $\times$ # people)$^{-1}$	fitted
σ	1/2	Unitless	assumed

4.6. Monte Carlo simulations and practical identifiability

To assess practical identifiability, we introduced Gaussian noise at levels of 0%, 1%, 5%, 10%, and 20% to the simulated data and evaluated the accuracy of parameter recovery under increasing uncertainty. The ARE is defined as [40]:

$$ARE(p_k) = 100\% \cdot \frac{1}{M} \sum_{j=1}^{M} \frac{\left|\hat{p}_k - p_k^j\right|}{\hat{p}_k},$$

where M is the number of Monte Carlo iterations, $\hat{p}_k$ is the estimated parameter value, and p_k^j is the j-th estimate obtained from the simulations. These ARE values provide a direct measure of how much noise impacts the practical identifiability of each parameter.

The results of the MCS are shown in Figure 3. Parameters such as δ_0, r_S, ν_i, and η exhibit high sensitivity to noise, as indicated by their increasing ARE values with higher noise levels. In contrast, parameters such as γ_I, γ_H, γ_A, and ν_h demonstrate more robust behavior with much lower ARE values across noise levels.

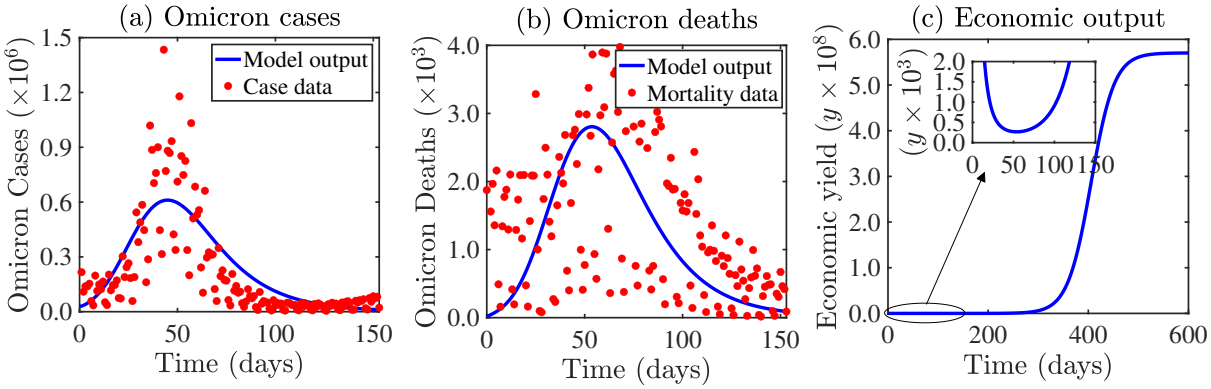

Figure 2. Model fit to daily COVID-19 case and mortality data for the US during the Omicron wave. Red dots represent observed data points, while solid blue curves denote model-generated estimates. (a) Fit to daily case data, showing the model's ability to capture infection trends. (b) Fit to daily mortality data, illustrating the agreement between observed and predicted deaths. (c) Economic yield over time, computed using the estimated parameters, highlighting the pandemic's economic impact.

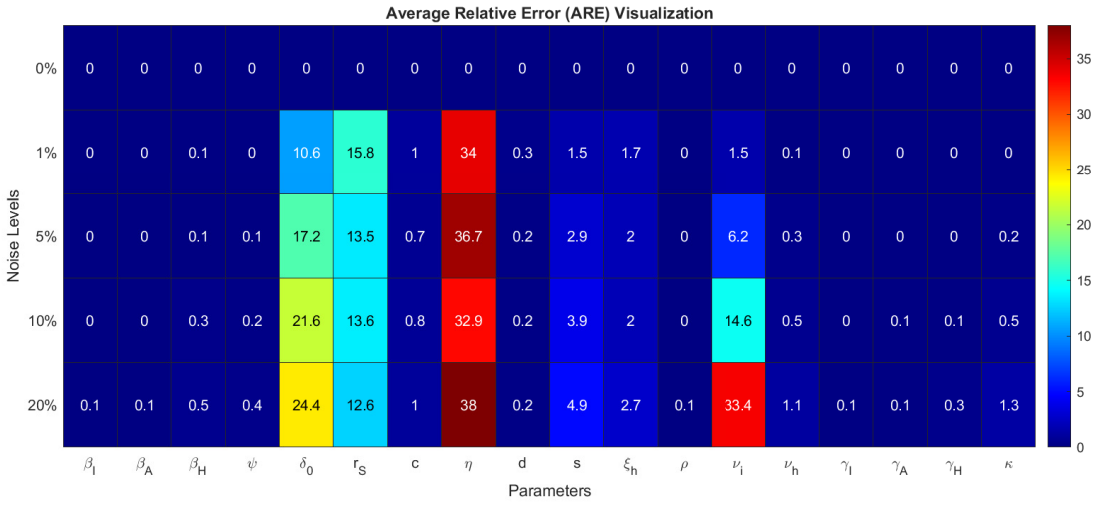

Figure 3. Heat map of Average Relative Error (ARE) values for key model parameters across noise levels with 1000 iterations.

The ARE analysis reveals important insights into parameter sensitivity. For example, β_I, representing the transmission rate of symptomatic individuals, remains robust at lower noise levels but experiences increased sensitivity at higher noise, with an ARE reaching 24.4% at 20% noise. The parameter δ_0, which reflects the social norm following rate, shows a sharp increase in sensitivity, from 10.6% at 1% noise to 24.4% at 20% noise. Parameters like r_S (cost of vaccination) and η (economic impact) are similarly sensitive, with r_S reaching 15.8% at 1% noise and 12.6% at 20% noise and η increasing from 34.0% at 1% noise to 38.0% at 20% noise.

Conversely, parameters such as ν_i and ν_h, representing death rates for symptomatic and hospitalized individuals, exhibit lower sensitivity to noise. For example, ν_i increases from 1.5% at 1% noise to 33.4% at 20% noise, whereas ν_h maintains much lower ARE values, reaching only 1.1% at 20% noise. These findings underscore the importance of practical identifiability assessments, as certain key parameters may require more precise data or refined modeling for reliable estimation. In contrast, others can be confidently estimated even in the presence of substantial noise.

4.7. 95% confidence intervals for estimated parameters

To quantify the uncertainty in parameter estimation, we computed the 95% confidence intervals (CIs) for all model parameters. These intervals were derived from the covariance matrix of the estimated parameters, obtained by evaluating the Jacobian of the residuals at the optimal solution using finite differences. A local linear approximation was assumed, and the resulting covariance matrix was used to generate 100 Monte Carlo samples drawn from a multivariate normal distribution. The model was then re-simulated for each sample to propagate the uncertainty and compute empirical confidence bounds.

Table 4. Estimated parameters with 95% confidence intervals.

Parameter	Median estimate	95% CI lower	95% CI upper
β_I	2.3600	2.1240	2.5960
β_A	0.4900	0.4410	0.5390
β_H	2.2600	2.0340	2.4860
ψ	0.0100	0.0090	0.0110
δ_0	0.3000	0.2700	0.3300
r_S	1.4900	1.3410	1.6390
c	1.9500	1.7550	2.1450
η	0.0300	0.0270	0.0330
d	2.9900	2.6910	3.2890
s	15.4300	13.8870	16.9730
ξ_h	16.3400	14.7060	17.9740
ρ	0.1700	0.1530	0.1870
ν_i	0.0200	0.0180	0.0220
ν_h	0.2100	0.1890	0.2310
γ_I	1.0000	0.9000	1.1000
γ_A	0.4200	0.3780	0.4620
γ_H	0.1500	0.1350	0.1650
κ	0.2200	0.1980	0.2420

Table 4 summarizes the median estimates of the model parameters and their associated 95% confidence intervals. This includes all epidemiological, behavioral, and economic parameters. Notably, the capital-related parameters in the last differential equation, such as the depreciation rate (d), the savings rate (s), and the health-related capital decay rate (ξ_h), were treated similarly and estimated alongside the other parameters using the same fitting procedure. Their inclusion within the same CI framework ensures the model's economic and epidemiological components are consistent.

5. Numerical simulation results

5.1. Assessing the sensitivity of the control reproduction number

Contour plots in Figure 4 illustrate the control reproduction number (R_c) "from Section 3.5 Eq (3.25)" as a function of vaccine efficacy (ε_V) and vaccine coverage (f_V). These plots assess the impact of control measures–such as masking, social distancing, and others–on reducing disease transmission through changes in the transmission rates ($\beta_I, \beta_A, \beta_H$). Additionally, they assess the impact of the proportion of symptomatic individuals post-incubation (ρ), and hospitalization timing via changes in the hospitalization rate (α) on R_c and explore how these changes influence the herd immunity thresholds. The proportion of symptomatic versus asymptomatic individuals in a population impacts disease control strategies by influencing transmission dynamics and detection capabilities. A higher proportion of asymptomatic cases may lead to undetected spread, necessitating broader surveillance and preventive measures, such as universal testing and contact tracing. Conversely, a higher symptomatic population may enable targeted interventions but may also overwhelm healthcare systems. Effective control requires adapting strategies to both the clinical manifestations of the disease and the hidden burden of asymptomatic carriers. Using the baseline parameters from Table 3, the basic reproduction number is ≈ 2.2, with a herd immunity threshold of $(1 - 1/2.2)/0.58 \approx 64\%$. For vaccines with efficacies of 65%, 75%, and 95%, the required coverage to reduce the reproduction number below one is 84%, 73%, and 57%, respectively (Figure 4(a),(e),(i)). Transmission-reducing measures that lower transmission by 20% and 60% reduce the thresholds to 50% (Figure 4(b)) and 28% (Figure 4(c)), reflecting reductions of 14% and 36% from the baseline. Conversely, a 20% increase in transmission raises the threshold to 72% (Figure 4(d)), an 8% increase. Reducing the proportion of individuals symptomatic post-incubation by 25% and 50% lowers the thresholds to 58% (Figure 4(f)) and 52% (Figure 4(g)), decreases of 6% and 12%. A 50% increase in this proportion raises the threshold by 8% (Figure 4(h)). Shortening the treatment-seeking time from 5 days to 1 and 3 days reduces the thresholds to 45% (Figure 4(i)) and 59% (Figure 4(j)), reductions of 19% and 5%. Extending the delay to 8 days increases the threshold by 3% (Figure 4(k)). In summary, effective vaccination, timely treatment, and transmission-reducing measures significantly lower R_c and herd immunity thresholds, highlighting the critical interplay between intervention strategies and disease control.

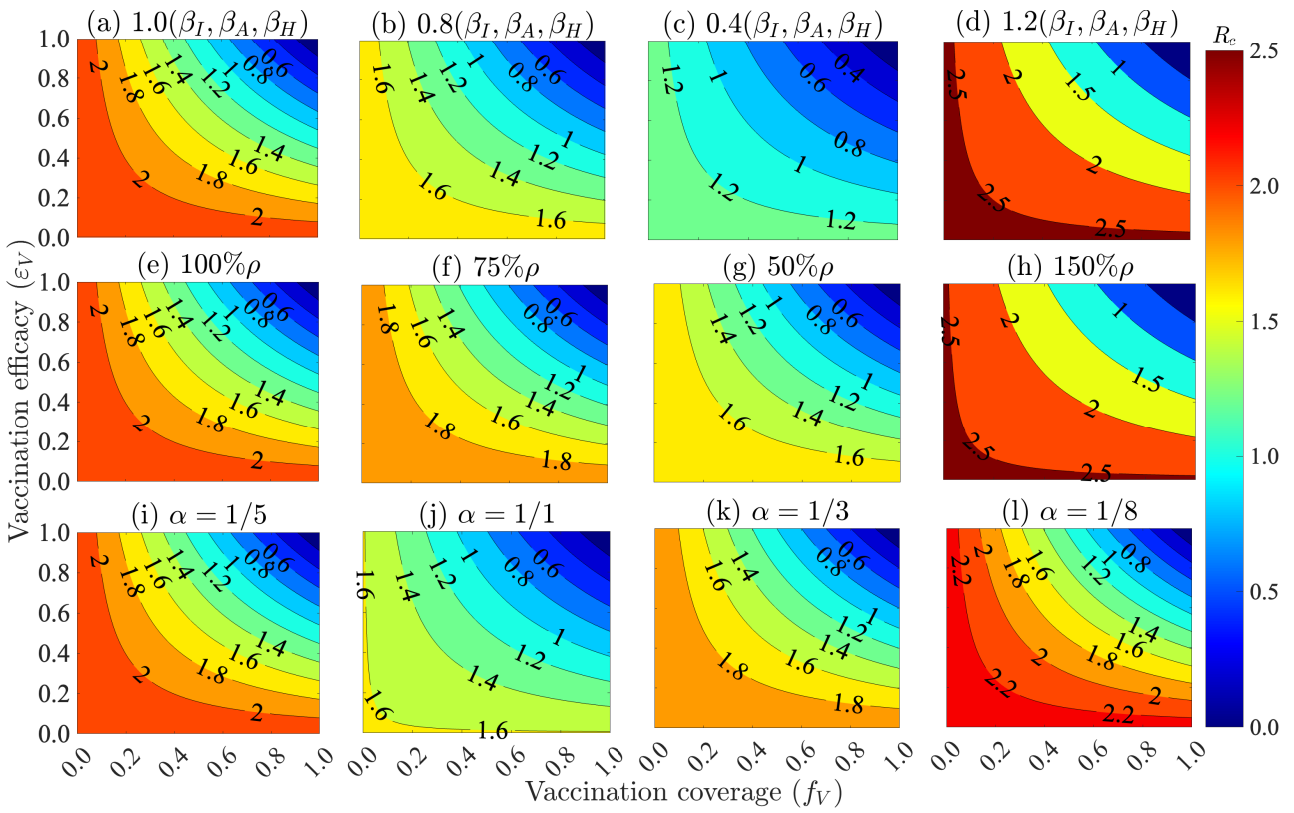

Figure 4. Contour plots depicting the control reproduction number (R_c) as a function of vaccine efficacy (ε_V) and coverage (f_V), highlighting the effects of (a)–(d): Transmission-reducing measures through changes in the transmission rates (β_I,β_A,β_H), (e)–(h): Symptomatic proportions (ρ), and (i)–(l): Hospitalization timing through changes in the hospitalization rate (α) on R_c and herd immunity thresholds. The parameters used are presented in Table 3.

5.2. *Assessing the impact of waning of vaccine-derived and natural immunity, the vaccination rate, and the recovery rate on daily disease and economic outcomes*

The time series analysis (Figure 5) demonstrates the effects of the waning vaccine-derived immunity rate (ω_V), waning natural immunity rate (ω_R), vaccination rate (ψ), and recovery rate of hospitalized individuals (γ_H) on infection incidence, mortality, and economic output. It should be noted that $1/\omega_V$ and $1/\gamma_H$ are the average duration of vaccine-derived immunity, natural immunity, and hospitalization, respectively. Baseline simulations using Model (2.1) parameters (Table 3) show that following Omicron's emergence, daily cases and deaths peak at 610,701 (day 45) and 2805 (day 54), respectively, (blue curves, Figure 5(a)–(h)). Shorter immunity durations delay and amplify peaks. In particular, 45-day vaccine-derived immunity (i.e., $1/\omega_V = 45$) shifts baseline daily peaks to days 66 for cases and 75 for deaths, with respective increases of 165% and 170% in baseline daily peak sizes, reducing economic output (magenta vs. blue curves, Figure 5(a),(e)). In contrast, a 6-month vaccine-derived immunity duration (i.e., $1/\omega_V = 180$) advances peaks by 3–4 days, lowering baseline daily case and death peaks by 14% and 15% (dotted light green vs. blue curves,

Figure 5(a),(e),(i)). A 1-year vaccine-derived immunity duration (i.e., $1/\omega_V = 365$) further shifts peaks earlier by 7 days, reducing cases and deaths by 25% and 26% (dark green vs. blue curves, Figure 5(a),(e)). Similar but smaller changes occur with waning natural immunity (Figure 5(b),(f)), with a 6-month duration altering baseline daily cases and deaths by 0.8% and 1.0%, and a 1-year duration by 1.1% and 1.3%. These results emphasize the need for durable immunity through sustained vaccine efficacy or booster doses. Higher vaccination rates (ψ) advance peak times and reduce peak magnitudes, while lower rates have the opposite effect. A 20% reduction in vaccination rate increases peak cases and deaths by 101% and 102%, delaying peaks by 7 and 6 days, respectively, and lowering economic yield (magenta vs. blue curves, Figure 5(c),(g),(k)). Conversely, a 20% increase in baseline vaccination reduces peak cases and deaths by 43% each, advancing peaks by 16 (cases) and 15 (deaths) days, with economic gains (dark green vs. blue curves, Figure 5(c),(g),(k)). This underscores the necessity of maintaining high vaccination coverage to mitigate health and economic impacts. Recovery rates of hospitalized individuals also significantly influence outcomes (Figure 5(d),(h),(l)). Lower recovery rates among hospitalized individuals heighten peak infections and deaths while reducing economic output. A 50% reduction in the baseline recovery rate of hospitalized individuals increases peak cases and deaths by 2.3% and 76%, respectively (magenta vs. blue curves, Figure 5(d),(h),(l)). In contrast, a 25% increase in the baseline of the recovery rate of hospitalized individuals reduces peaks by 0.7% (cases) and 18% (deaths), enhancing economic output (dotted light green vs. blue curves, Figure 5(d),(h),(l)). A 50% increase in the baseline of recovery rate of hospitalized individuals further lowers peak cases and deaths by 1.3% and 31% (dark green vs. blue, Figure 5(d),(h),(l)). These results highlight the importance of optimizing recovery rates to reduce emerging variants' public health and economic burden.

5.3. Assessing the impact of transmission reduction measures, vaccine efficacy, time to seek treatment, and the proportion of symptomatic infectious individuals on cumulative cases and deaths

Figure 6 presents cumulative Omicron cases (Figure 6(a)–(d)) and deaths (Figure 6(e)–(h)) over time under varying transmission rates ($\beta \in \{\beta_A, \beta_I, \beta_H\}$), vaccine efficacy ($\varepsilon_V$), hospitalization rates (α) or average time to seek treatment ($1/\alpha$), and proportions of symptomatic infectious individuals (ρ). The results indicate that one month after the Omicron variant's onset, the baseline cumulative cases and deaths are 60,424,400 and 157,656, respectively (blue curves, Figure 6). A 10% increase in transmission rate raises cases by 65% and deaths by 51% (early portion of blue vs. magenta curves, Figure 6(a),(e)), while a 10% reduction lowers cases by 40% and deaths by 33% (blue vs. green curves). Suppose the Omicron variant is extended by over a year. In that case, baseline cumulative cases and deaths are projected to have increased to 365,498,000 and 1,798,540, respectively, with a 10% transmission increase leading to 116% and 113% rises in cases and deaths, respectively. In contrast, a 10% reduction results in 62% and 60% decreases. This underscores the role of non-pharmaceutical interventions like mask mandates and social distancing in reducing infections and fatalities. A 10% decrease in vaccine efficacy raises cases by 18% and deaths by 12% (blue vs. magenta curves, Figure 6(b),(f)), whereas a 10% increase reduces cases by 15% and deaths by 10% (blue vs. green curves) after one month. Over a year, these changes amplify, with a 10% efficacy reduction increasing cases by 137% and deaths by 134%, and a 10% increase decreasing cases by 50% and deaths by 49%. This highlights the importance of booster campaigns and updated vaccines

in mitigating disease burden. Regarding hospitalization, delays (early interventions) lead to higher (lower) cumulative cases and deaths (Figure 6(c),(g)), emphasizing the role of healthcare capacity and timely treatment in reducing mortality. Similarly, a lower proportion of symptomatic infectious individuals decreases cumulative cases and deaths, while a higher proportion increases them. Specifically, a 10% reduction in ρ decreases cases by 17% and deaths by 22% (blue vs. green curves, Figure 6(d),(h)), whereas a 10% increase raises cases by 20% and deaths by 27% (blue vs. magenta curves) after one month. Over a year, a 10% decrease in ρ leads to a 28% and 35% reduction in cases and deaths, while a 10% increase results in 36% and 49% rises. This suggests that while increased symptom presentation aids detection, it also amplifies transmission, necessitating rapid testing and isolation strategies. Overall, reducing transmission, enhancing vaccine efficacy, increasing hospitalization capacity, and managing symptomatic cases are crucial to minimizing Omicron-related cases and deaths. Public health measures should prioritize vaccination, early detection, and resource allocation to mitigate severe outcomes.

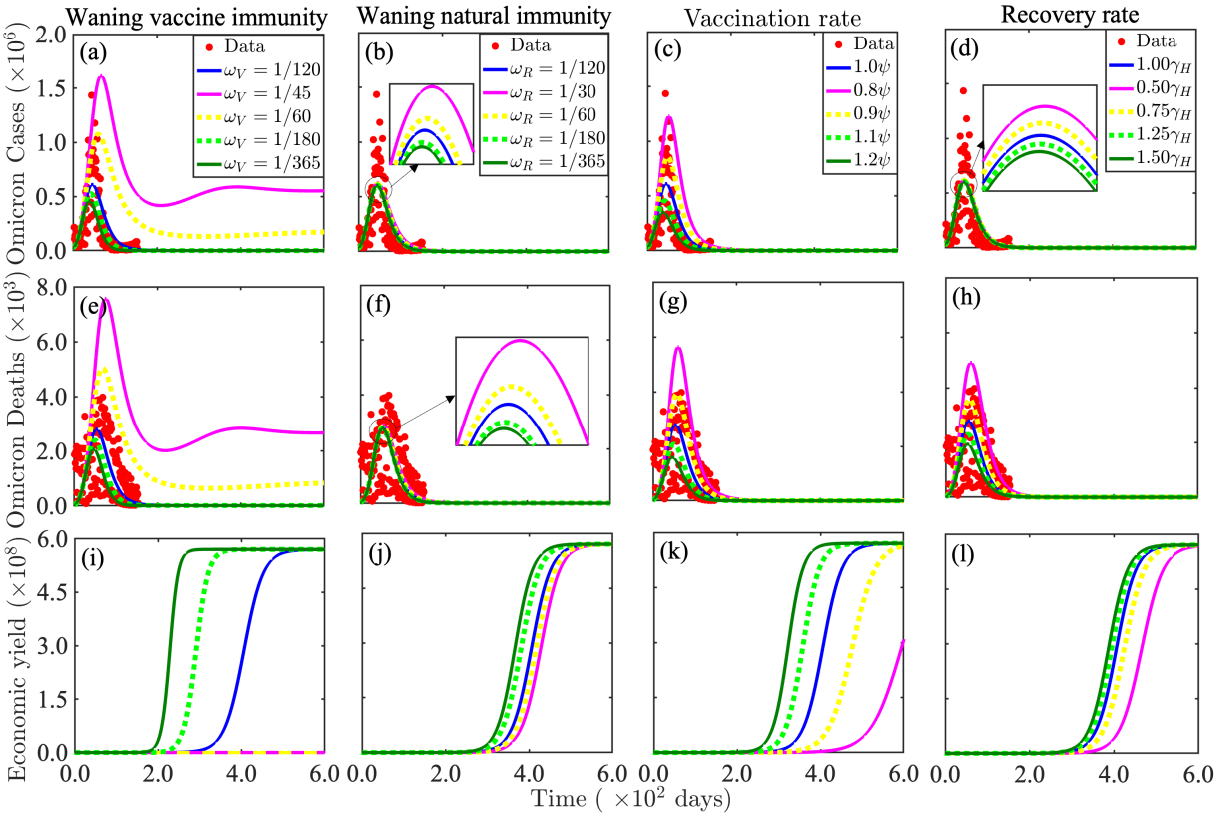

Figure 5. Local sensitivity analysis of the vaccine-derived immunity waning rate (ω_V) or the average vaccine-derived immunity duration ($1/\omega_V$) ((a), (e), and (i)), the natural immunity waning rate (ω_R) or the average duration of natural immunity ($1/\omega_R$) ((b), (f), and (j)), the vaccination rate (ψ) ((c), (g), and (k)), and the recovery rate (γ_H) or the average duration of hospitalization ($1/\gamma_H$) ((d), (h), and (l)), on daily Omicron cases ((a)–(d)), Omicron deaths ((e)–(h)), and economic yield ((i)–(l)). Other parameters and the initial conditions used for the simulations are presented in Table 3.

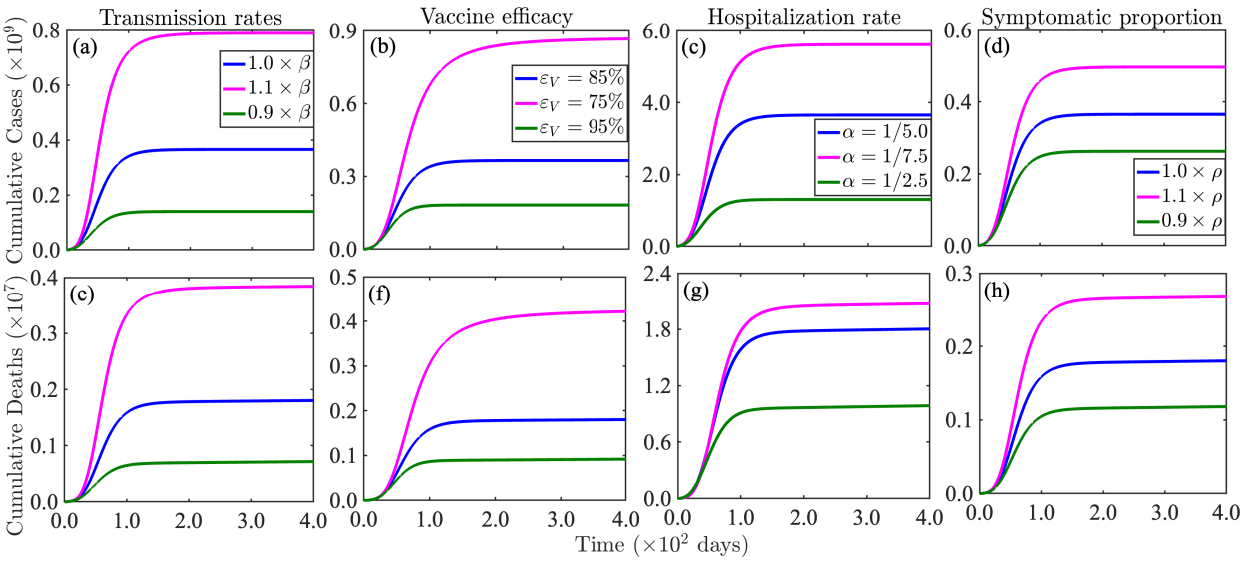

Figure 6. Local sensitivity analysis of the transmission rates ($\beta \in \{\beta_A, \beta_I, \beta_H\}$) ((a) and (e), the efficacy of vaccines (ε_V) ((b), (f)), the hospitalization rate vaccination rate (α) ((c) and (g)), and the proportion of symptomatic infectious humans (ρ) ((d) and (h)), on the cumulative Omicron cases ((a)–(d)) and the cumulative Omicron deaths ((e)–(h)). Other parameters used for the simulations are presented in Table 3.

5.4. Global sensitivity analysis

A global sensitivity analysis is a crucial step in any mathematical modeling study as it enables identifying the most influential parameters that affect the model's response functions. This analysis provides valuable insight into which variables most strongly impact the outcomes, helping to prioritize areas for intervention and refine model predictions. By quantifying the uncertainty in model outputs due to variability in input parameters, it ensures that the conclusions drawn are robust and reliable. For complex systems such as infectious disease dynamics, sensitivity analysis also highlights the interactions between parameters, revealing how changes in one factor may influence others, thereby guiding more effective and targeted interventions. In this study, a global sensitivity analysis was carried out for the model (2.1) using the Latin Hypercube Sampling (LHS) and Partial Rank Correlation Coefficient (PRCC) approach [42]. This approach assessed the impact of various model parameters on two key response functions: Omicron incidence and Omicron deaths. A uniform distribution was assumed for each parameter, and simulations were run with 1000, 5000, and 10,000 different sets of parameters. Since the results for 10,000 simulations were similar to those for the other cases, the results for 10,000 simulations were retained. The analysis (depicted in Figure 7) reveals that changes in vaccine efficacy (ε_V), vaccine-derived immunity duration (ω_V), symptomatic individual transmission rate (β_I), and vaccination rate (ψ) had the most significant impact on both response functions, with PRCCs greater than 0.6. Specifically, increases in ε_V and ψ will trigger significant reductions in both Omicron incidence and deaths, while increases in β_I and ω_V will result in substantial increases in both response functions. These results suggest that increasing vaccination coverage and using vaccines with high efficacy can significantly reduce both the number of infections

and deaths, while shorter vaccine-derived immunity durations and higher transmission from symptomatic individuals may exacerbate the situation. Additionally, changes in the transmission rate of asymptomatic individuals (β_A) leads to notable changes in both response functions, though to a lesser extent. Variation in the hospitalization rate (α), the recovery rate from infection (γ_H), and the proportion of symptomatic individuals at the end of the incubation period (ρ) primarily impact Omicron-related deaths, notably, but have a limited effect on the number of cases. These findings emphasize the importance of controlling symptomatic transmission, extending vaccine efficacy, and enhancing vaccination rates to mitigate the broader impact of COVID-19. The public health implication of these results is that interventions aimed at increasing vaccination efficacy and coverage, while reducing symptomatic transmission, are likely to have the most substantial impact on both case numbers and mortality. In contrast, focusing on parameters that only affect mortality may be less effective in controlling overall disease spread.

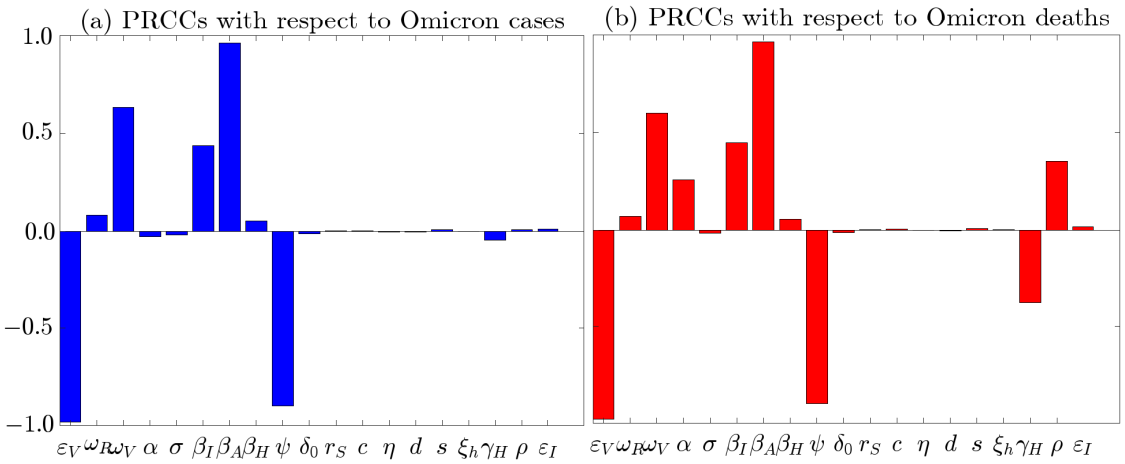

Figure 7. Global sensitivity analysis of model parameters on Omicron (a) incidence and (b) deaths using the Latin hypercube sampling (LHS) and partial rank correlation coefficient (PRCC) approach. The analysis reveals that vaccine efficacy (ε_V), vaccination rate (ψ), symptomatic individual transmission rate (β_I), and vaccine-derived immunity duration (ω_V) significantly impact both response functions, with increases in ε_V and ψ reducing incidence and deaths, while higher β_I and shorter ω_V exacerbate both. Asymptomatic transmission rate (β_A) and parameters affecting hospitalization and recovery primarily influence deaths, emphasizing the importance of improving vaccination coverage and efficacy to control COVID-19 spread and mortality. The parameters used are presented in Table 3.

6. Discussion and conclusions

6.1. Discussion

W present a comprehensive mathematical model that integrates human population dynamics, COVID-19 epidemiology, vaccination behavior through imitation dynamics, and the economic impact of the disease using neoclassical economic growth theory to examine COVID-19 transmission and control in the US. The model incorporates key epidemiological and economic interactions to provide

a holistic understanding of disease spread and intervention effectiveness. Reproduction numbers under various conditions are derived to analytically assess the existence and stability of multiple disease-free equilibria. Furthermore, we investigate the conditions leading to endemic equilibria, offering critical insights into long-term disease persistence and control strategies. The model is fitted to daily case and mortality data for the Omicron variant in the US, and the parameterized model is used to evaluate various intervention scenarios.

The findings underscore the critical role of vaccination efficacy, coverage, and complementary interventions in controlling disease transmission. The observed reductions in herd immunity thresholds with improved vaccine efficacy and timely treatment align with previous studies emphasizing the synergistic effect of vaccination and non-pharmaceutical interventions (NPIs) on R_c suppression [25, 43–45]. The proportion of symptomatic versus asymptomatic individuals affects disease control by influencing transmission and detection. A higher asymptomatic proportion may lead to undetected spread, requiring broader surveillance and preventive measures, such as universal testing. Conversely, more symptomatic cases enable targeted interventions but may strain healthcare systems. Effective control strategies must balance both clinical manifestations and the hidden burden of asymptomatic carriers. Our results show that reductions in symptomatic proportions and hospitalization delays further highlight the importance of targeted strategies to optimize healthcare responses, consistent with results from modeling studies exploring time-sensitive interventions [46, 47]. Conversely, increased transmission or delayed treatment exacerbates control efforts, reinforcing the necessity of robust and multi-faceted approaches. These insights contribute to a broader understanding of epidemic control dynamics, complementing theoretical and empirical frameworks in the literature. Achieving high vaccine coverage during the COVID-19 pandemic was critical for controlling the disease, but was hindered by widespread vaccine hesitancy, misinformation, and political factors, despite its proven importance in reducing transmission [48, 49]. While higher vaccine coverage would have lowered herd immunity thresholds and reduced the burden on healthcare systems, the waning of vaccine-derived immunity further complicated the issue, requiring continuous efforts to maintain high coverage. Ultimately, robust and sustained vaccination efforts and complementary interventions were essential to mitigating health and economic impacts.

This study highlights the critical role of immunity duration, vaccination rates, and hospitalization recovery in shaping COVID-19 dynamics and economic outcomes. Our results demonstrate that shorter vaccine-derived and natural immunity durations amplify and delay infection and mortality peaks, whereas longer-lasting immunity reduces peak magnitudes and advances their timing. These findings underscore the importance of durable immunity, either through sustained vaccine efficacy or timely booster doses, to mitigate the impact of emerging variants. Prior research has similarly emphasized the benefits of long-lasting immunity in controlling outbreaks and minimizing severe outcomes [10, 50, 51]. Vaccination rates also significantly influence epidemic trajectories, with higher coverage reducing peak cases and deaths while improving economic performance. Conversely, reductions in vaccination rates lead to prolonged outbreaks and economic downturns, reinforcing the necessity of maintaining high vaccine uptake. These findings highlight the fact that vaccination is a key strategy in pandemic control. However, achieving high vaccination rates during the COVID-19 pandemic has been challenging, primarily due to vaccine hesitancy, which has been exacerbated by misinformation, political factors, and distrust in public health systems [52, 53]. This hesitancy has hindered efforts to reach ID-19. Our findings emphasize the importance of addressing these barriers to

improve vaccination uptake and mitigate both the health and economic consequences of future pandemics. Similarly, hospitalization recovery rates play a crucial role in disease burden and economic resilience. Faster recovery reduces mortality and economic losses, while slower recovery exacerbates strain on healthcare systems. Hence, the study demonstrates that optimizing hospital treatment capacity can significantly mitigate both direct health consequences and broader economic disruptions. Overall, these results emphasize the need for sustained immunity, widespread vaccination, and improved healthcare capacity to minimize the health and economic burden of future COVID-19 waves and emerging variants. Policy interventions that enhance vaccine durability, ensure consistent vaccination efforts, and improve hospital recovery rates can play a crucial role in pandemic management.

Furthermore, the findings of the study highlight the significant impact of transmission rates, vaccine efficacy, hospitalization dynamics, and symptomatic case proportions on the cumulative burden of Omicron-related cases and deaths. Higher transmission rates substantially increase infections and fatalities over both short- and long-term periods, underscoring the effectiveness of non-pharmaceutical interventions such as mask mandates and social distancing in curbing virus spread, consistent with previous studies [54]. Vaccine efficacy plays a crucial role, with lower efficacy leading to increased cases and deaths, reinforcing the importance of booster campaigns and updated vaccines, as supported by reports on waning immunity and variant-specific vaccine responses [55]. Timely hospitalization is another critical factor, as delays exacerbate disease outcomes, aligning with prior studies emphasizing the role of healthcare system capacity in pandemic management [56]. Additionally, a higher proportion of symptomatic individuals increases transmission despite aiding case detection, highlighting the need for rapid testing and isolation strategies to balance disease control and surveillance efforts [57]. Collectively, these findings emphasize the importance of comprehensive public health strategies, including vaccination, early detection, and healthcare preparedness, in minimizing the burden of Omicron and future variants.

The global sensitivity analysis conducted in this study underscores the importance of key parameters, such as vaccine efficacy (ε_V), vaccination rate (ψ), and symptomatic transmission (β_I), in controlling Omicron incidence and mortality. These findings emphasize the central role of high vaccine coverage and efficacy in reducing both disease spread and mortality. The results suggest that strategies to enhance vaccination rates and vaccine efficacy while minimizing symptomatic transmission could substantially impact both health outcomes and economic recovery. In contrast, focusing on aspects like the time that elapses from symptom onset or identification before seeking treatment (or the hospitalization rate) or asymptomatic transmission may be less effective in curbing disease transmission and mortality. Thus, targeted public health interventions aimed at increasing vaccine effectiveness and coverage are critical for effective pandemic control.

6.2. Concluding remarks

This study underscores the critical role of immunity duration, vaccination rates, and healthcare capacity in mitigating the health and economic impacts of COVID-19. Through sustained vaccine efficacy or timely booster doses, durable immunity reduces infection peaks and mortality, highlighting the need for long-term immunization strategies. High vaccination coverage minimizes outbreaks and economic downturns, reinforcing the urgency of addressing vaccine hesitancy through targeted public health efforts. Efficient hospitalization recovery alleviates healthcare strain and economic losses,

emphasizing the importance of strengthening treatment capacity. Moreover, non-pharmaceutical interventions remain essential in curbing transmission, particularly in the face of waning immunity and emerging variants. Ultimately, a multi-pronged approach–integrating sustained vaccination, rapid case detection, and robust healthcare infrastructure–is crucial for effective pandemic control and preparedness.

6.3. Future research directions

In the future, researchers should explicitly address two critical extensions to enhance policy relevance.

First, modeling detailed policy interventions, including specific lockdown durations and varying intensities of economic restrictions, would illuminate the interactions between public health measures and economic outcomes. Such an analysis could clearly identify trade-offs and feedback loops between disease dynamics and economic activities.

Second, incorporating government borrowing capacities, particularly by examining interest rates as indicators of policy deployment capability, offers another significant research direction. Analyzing borrowing costs in relation to economic capacity would better reflect real-world policy strategies and improve the practical applicability of the model.

Both extensions require considerable model modifications and analyses, providing valuable avenues for subsequent investigation.

Use of AI tools declaration

The authors declare they have not used Artificial Intelligence (AI) tools in the creation of this article.

Conflict of interest

Maia Martcheva is a guest editor for [Mathematical Biosciences and Engineering] and was not involved in the editorial review or the decision to publish this article. The authors declare there is no conflict of interest.

References

1. U.S. deaths from COVID-19, Worldometer, 2025. Available from: https://www.worldometers.info/coronavirus/country/us/#google_vignette.
2. L. L. O'Mahoney, A. Routen, C. Gillies, W. Ekezie, A. Welford, A. Zhang, et al., The prevalence and long-term health effects of long covid among hospitalised and non-hospitalised populations: A systematic review and meta-analysis, *eClinicalMedicine*, **55** (2023), 101762. https://doi.org/10.1016/j.eclinm.2022.101762
3. R. Filip, R. G. Puscaselu, L. Anchidin-Norocel, M. Dimian, W. K. Savage, Global challenges to public health care systems during the COVID-19 pandemic: A review of pandemic measures and problems, *J. Pers. Med.*, **12** (2022), 1295. https://doi.org/10.3390/jpm12081295

4. E. A. Andraska, O. Alabi, C. Dorsey, Y. Erben, G. Velazquez, C. Franco-Mesa, et al., Health care disparities during the COVID-19 pandemic, *Semin. Vasc. Surg.*, **34** (2021), 82–88. https://doi.org/10.1053/j.semvascsurg.2021.08.002
5. S. Naseer, S. Khalid, S. Parveen, K. Abbass, H. Song, M. V. Achim, COVID-19 outbreak: Impact on global economy, *Front. Public Health*, **10** (2023), 1009393. https://doi.org/10.3389/fpubh.2022.1009393
6. Z. Xu, A. Elomri, L. Kerbache, A. El Omri, Impacts of COVID-19 on global supply chains: Facts and perspectives, *IEEE Eng. Manage. Rev.*, **48** (2020), 153–166. https://doi.org/10.1109/EMR.2020.3018420
7. D. Vasireddy, P. Atluri, S. V. Malayala, R. Vanaparthy, G. Mohan, Review of COVID-19 vaccines approved in the United States of America for emergency use, *J. Clin. Med. Res.*, **13** (2021), 204–213. https://doi.org/10.14740/jocmr4490
8. A. L. Beatty, N. D. Peyser, X. E. Butcher, J. M. Cocohoba, F. Lin, J. E. Olgin, et al., Analysis of COVID-19 vaccine type and adverse effects following vaccination, *JAMA Netw. Open*, **4** (2021), e2140364. https://doi.org/10.1001/jamanetworkopen.2021.40364
9. F. P. Polack, S. J. Thomas, N. Kitchin, J. Absalon, A. Gurtman, S. Lockhart, et al., Safety and efficacy of the BNT162b2 mRNA COVID-19 vaccine, *N. Engl. J. Med.*, **383** (2020), 2603–2615. https://doi.org/10.1056/NEJMoa2034577
10. S. M. Moghadas, T. N. Vilches, K. Zhang, C. R. Wells, A. Shoukat, B. H. Singer, et al., The impact of vaccination on coronavirus disease 2019 (COVID-19) outbreaks in the United States, *Clin. Infect. Dis.*, **73** (2021), 2257–2264. https://doi.org/10.1093/cid/ciab079
11. P. B. Gilbert, D. C. Montefiori, A. B. McDermott, Y. Fong, D. Benkeser, W. Deng, et al., Immune correlates analysis of the mRNA-1273 COVID-19 vaccine efficacy clinical trial, *Science*, **375** (2022), 43–50. https://doi.org/10.1126/science.abm3425
12. H. J. Larson, E. Gakidou, C. J. L. Murray, The vaccine-hesitant moment, *N. Engl. J. Med.*, **387** (2022), 58–65. https://doi.org/10.1056/NEJMra2106441
13. Communicating with patients about COVID-19 vaccination, World Health Organization, 2021. Available from: https://iris.who.int/bitstream/handle/10665/340751/WHO-EURO-2021-2281-42036-57837-eng.pdf.
14. J. Khubchandani, S. Sharma, J. H. Price, M. J. Wiblishauser, M. Sharma, F. J. Webb, COVID-19 vaccination hesitancy in the United States: A rapid national assessment, *J. Community Health*, **46** (2021), 270–277. https://doi.org/10.1007/s10900-020-00958-x
15. G. Troiano, A. Nardi, Vaccine hesitancy in the era of COVID-19, *Public Health*, **194** (2021), 245–251. https://doi.org/10.1016/j.puhe.2021.02.025
16. D. Danelski, COVID-19 lockdowns reduced disease spread but with costs, in *UCR School of Business News*, 2023. Available from: https://business.ucr.edu/news/2023/03/07/covid-lockdowns-reduced-disease-spread.

17. J. J. V. Bavel, K. Baicker, P. S. Boggio, V. Capraro, A. Cichocka, M. Cikara, et al., Using social and behavioural science to support COVID-19 pandemic response, *Nat. Hum. Behav.*, **4** (2020), 460–471. https://doi.org/10.1038/s41562-020-0884-z

18. N. M. Ferguson, D. Laydon, G. Nedjati-Gilani, N. Imai, K. Ainslie, M. Baguelin, et al., Report 9: Impact of non-pharmaceutical interventions (NPIs) to reduce COVID-19 mortality and healthcare demand, in *Imperial College COVID-19 Response Team*, **2020** (2020), 1–20. https://doi.org/10.25561/77482

19. C. N. Ngonghala, E. Iboi, S. Eikenberry, M. Scotch, C. R. MacIntyre, M. H. Bonds, et al., Mathematical assessment of the impact of non-pharmaceutical interventions on curtailing the 2019 novel coronavirus, *Math. Biosci.*, **325** (2020), 108364. https://doi.org/10.1016/j.mbs.2020.108364

20. C. N. Ngonghala, E. Iboi, A. B. Gumel, Could masks curtail the post-lockdown resurgence of COVID-19 in the US?, *Math. Biosci.*, **329** (2020), 108452. https://doi.org/10.1016/j.mbs.2020.108452

21. C. N. Ngonghala, J. R. Knitter, L. Marinacci, M. H. Bonds, A. B. Gumel, Assessing the impact of widespread respirator use in curtailing COVID-19 transmission in the USA, *R. Soc. Open Sci.*, **8** (2021), 210699. https://doi.org/10.1098/rsos.210699

22. A. B. Gumel, E. A. Iboi, C. N. Ngonghala, E. H. Elbasha, A primer on using mathematics to understand COVID-19 dynamics: Modeling, analysis and simulations, *Infect. Dis. Modell.*, **6** (2021), 148–168. https://doi.org/10.1016/j.idm.2020.11.005

23. E. A. Iboi, C. N. Ngonghala, A. B. Gumel, Will an imperfect vaccine curtail the COVID-19 pandemic in the U.S.?, *Infect. Dis. Modell.*, **5** (2020), 510–524. https://doi.org/10.1016/j.idm.2020.07.006

24. A. B. Gumel, E. A. Iboi, C. N. Ngonghala, G. A. Ngwa, Toward achieving a vaccine-derived herd immunity threshold for COVID-19 in the U.S., *Front. Public Health*, **9** (2021), 709369. https://doi.org/10.3389/fpubh.2021.709369

25. C. N. Ngonghala, H. B. Taboe, S. Safdar, A. B. Gumel, Unraveling the dynamics of the Omicron and Delta variants of the 2019 coronavirus in the presence of vaccination, mask usage, and antiviral treatment, *Appl. Math. Modell.*, **114** (2023), 447–465. https://doi.org/10.1016/j.apm.2022.09.017

26. A. Alsammani, Mathematical analysis of autonomous and nonautonomous hepatitis B virus transmission models, in *International Conference on Computational Science and Its Applications*, Springer, (2023), 327–343. https://doi.org/10.1007/978-3-031-37108-0_21

27. C. N. Ngonghala, P. Goel, D. Kutor, S. Bhattacharyya, Human choice to self-isolate in the face of the COVID-19 pandemic: A game dynamic modelling approach, *J. Theor. Biol.*, **521** (2021), 110692. https://doi.org/10.1016/j.jtbi.2021.110692

28. M. Martcheva, N. Tuncer, C. N. Ngonghala, Effects of social-distancing on infectious disease dynamics: An evolutionary game theory and economic perspective, *J. Biol. Dyn.*, **15** (2021), 342–366. https://doi.org/10.1080/17513758.2021.1946177

29. N. Banholzer, E. Van Weenen, A. Lison, A. Cenedese, A. Seeliger, B. Kratzwald, et al., Estimating the effects of non-pharmaceutical interventions on the number of new infections with COVID-19 during the first epidemic wave, *PLoS One*, **16** (2021), e0252827. https://doi.org/10.1371/journal.pone.0252827

30. M. L. Diagne, H. Rwezaura, S. Y. Tchoumi, J. M. Tchuenche, A mathematical model of COVID-19 with vaccination and treatment, *Comput. Math. Methods Med.*, **2021** (2021), 1250129. https://doi.org/10.1155/2021/1250129

31. R. M. Solow, A contribution to the theory of economic growth, *Q. J. Econ.*, **70** (1956), 65–94. https://doi.org/10.2307/1884513

32. T. W. Swan, Economic growth and capital accumulation, *Econ. Rec.*, **32** (1956), 334–361. https://doi.org/10.1111/j.1475-4932.1956.tb00434.x

33. C. W. Cobb, P. H. Douglas, A theory of production, *Am. Econ. Rev.*, **18** (1928), 139–165. Available from: https://www.jstor.org/stable/1811556.

34. A. L. Lloyd, Realistic distributions of infectious periods in epidemic models: changing patterns of persistence and dynamics, *Theor. Popul. Biol.*, **60** (2001), 59–71. https://doi.org/10.1006/tpbi.2001.1525

35. A. L. Lloyd, Destabilization of epidemic models with the inclusion of realistic distributions of infectious periods, *Proc. Roy. Soc. Lond. B*, **268** (2001), 985–993. https://doi.org/10.1098/rspb.2001.1599

36. P. J. Lu, T. Zhou, T. A. Santibanez, A. Jain, C. L. Black, A. Srivastav, et al., COVID-19 bivalent booster vaccination coverage and intent to receive booster vaccination among adolescents and adults—United States, November–December 2022, *Morb. Mortal. Wkly. Rep.*, **72** (2023), 190–198. https://doi.org/10.15585/mmwr.mm7207a5

37. C. Willyard, How quickly does COVID immunity fade? What scientists know, *Nature*, **614** (2023), 395–396. https://doi.org/10.1038/d41586-023-00124-y

38. N. Prasad, G. Derado, S. A. Nanduri, H. E. Reses, H. Dubendris, E. Wong, et al., Effectiveness of a COVID-19 additional primary or booster vaccine dose in preventing SARS-CoV-2 infection among nursing home residents during widespread circulation of the Omicron variant, United States, February 14 March 27, 2022, *Morb. Mortal. Wkly. Rep.*, **71** (2022), 633–637. https://doi.org/10.15585/mmwr.mm7118a4

39. S. Safdar, C. N. Ngonghala, A. B. Gumel, Mathematical assessment of the role of waning and boosting immunity against the BA.1 Omicron variant in the United States, *Math. Biosci. Eng.*, **20** (2023), 179–212. https://doi.org/10.3934/mbe.2023009

40. N. Tuncer, A. Timsina, M. Nuno, G. Chowell, M. Martcheva, Parameter identifiability and optimal control of an SARS-CoV-2 model early in the pandemic, *J. Biol. Dyn.*, **16** (2022), 412–438. https://doi.org/10.1080/17513758.2022.2078899

41. Centers for Disease Control and Prevention, U.S. life expectancy declined to 77.0 years in 2020, 2022. Available from: https://www.cdc.gov/nchs/pressroom/nchs_press_releases/2022/20220831.htm.

42. A. Saltelli, M. Ratto, T. Andres, F. Campolongo, J. Cariboni, D. Gatelli, et al., *Global Sensitivity Analysis: The primer*, John Wiley & Sons, 2008. https://doi.org/10.1002/9780470725184

43. R. M. Anderson, *Infectious Diseases of Humans: Dynamics and Control*, Oxford University Press, 1991. https://doi.org/10.1093/oso/9780198545996.001.0001

44. S. Moore, E. M. Hill, M. J. Tildesley, L. Dyson, M. J. Keeling, Vaccination and non-pharmaceutical interventions for COVID-19: A mathematical modelling study, *Lancet Infect. Dis.*, **21** (2021), 793–802. https://doi.org/10.1016/S1473-3099(21)00143-2

45. A. D. Paltiel, J. L. Schwartz, A. Zheng, R. P. Walensky, Clinical outcomes of a COVID-19 vaccine: Implementation over efficacy, *Health Aff.*, **40** (2021), 42–52. https://doi.org/10.1377/hlthaff.2020.02054

46. M. E. Kretzschmar, G. Rozhnova, M. C. J. Bootsma, M. van Boven, J. H. H. M. van de Wijgert, M. J. M. Bonten, Impact of delays on effectiveness of contact tracing strategies for COVID-19: A modelling study, *Lancet Public Health*, **5** (2020), e452–e459. https://doi.org/10.1016/S2468-2667(20)30157-2

47. N. C. Grassly, C. Fraser, Mathematical models of infectious disease transmission, *Nat. Rev. Microbiol.*, **6** (2008), 477–487. https://doi.org/10.1038/nrmicro1845

48. T. Zimmerman, K. Shiroma, K. R. Fleischmann, B. Xie, C. Jia, N. Verma, et al., Misinformation and COVID-19 vaccine hesitancy, *Vaccine*, **41** (2023), 136–144. https://doi.org/10.1016/j.vaccine.2022.11.014

49. S. Loomba, A. De Figueiredo, S. J. Piatek, K. De Graaf, H. J. Larson, Measuring the impact of COVID-19 vaccine misinformation on vaccination intent in the UK and USA, *Nat. Hum. Behav.*, **5** (2021), 337–348. https://doi.org/10.1038/s41562-021-01056-1

50. F. Menegale, M. Manica, A. Zardini, G. Guzzetta, V. Marziano, V. d'Andrea, et al., Evaluation of waning of SARS-CoV-2 vaccine-induced immunity: A systematic review and meta-analysis, *JAMA Netw. Open*, **6** (2023), e2310650. https://doi.org/10.1001/jamanetworkopen.2023.10650

51. C. Caetano, M. L. Morgado, P. Patrício, A. Leite, A. Machado, A. Torres, et al., Measuring the impact of COVID-19 vaccination and immunity waning: A modelling study for Portugal, *Vaccine*, **40** (2022), 7115–7121. https://doi.org/10.1016/j.vaccine.2022.10.007

52. J. G. Lu, Two large-scale global studies on COVID-19 vaccine hesitancy over time: Culture, uncertainty avoidance, and vaccine side-effect concerns, *J. Pers. Social Psychol.*, **124** (2023), 683–706. https://doi.org/10.1037/pspa0000320

53. M. Sallam, COVID-19 vaccine hesitancy worldwide: A concise systematic review of vaccine acceptance rates, *Vaccines*, **9** (2021), 160. https://doi.org/10.3390/vaccines9020160

54. J. M. Brauner, S. Mindermann, M. Sharma, D. Johnston, J. Salvatier, T. Gavenčiak, et al., Inferring the effectiveness of government interventions against COVID-19, *Science*, **371** (2021), eabd9338. https://doi.org/10.1126/science.abd9338

55. N. Andrews, J. Stowe, F. Kirsebom, S. Toffa, T. Rickeard, E. Gallagher, et al., COVID-19 vaccine effectiveness against the Omicron (B.1.1.529) variant, *N. Engl. J. Med.*, **386** (2022), 1532–1546. https://doi.org/10.1056/NEJMoa2119451

56. A. B. Hogan, B. L. Jewell, E. Sherrard-Smith, J. F. Vesga, O. J. Watson, C. Whittaker, et al., Potential impact of the COVID-19 pandemic on HIV, tuberculosis, and malaria in low-income and middle-income countries: A modelling study, *Lancet Global Health*, **8** (2020), E1132–E1141. https://doi.org/10.1016/S2214-109X(20)30288-6

57. M. A. Johansson, T. M. Quandelacy, S. Kada, P. V. Prasad, M. Steele, J. T. Brooks, et al., SARS-CoV-2 transmission from people without COVID-19 symptoms, *JAMA Netw. Open*, **4** (2021), e2035057. https://doi.org/10.1001/jamanetworkopen.2020.35057

AIMS Press